

97

**THE CRYSTAL STRUCTURE ANALYSIS OF
C₂₈H₂₄N₂O₄ AND C₂₃H₃₂N₄Se BY SINGLE
CRYSTAL X-RAY DIFFRACTION TECHNIQUE**

**A Thesis Submitted to the
Graduate School of Natural and Applied Sciences of
Dokuz Eylül University
In Partial Fulfillment of the Requirements for
The Degree of Master of Science in Physics**

**T.C. YÜKSEKÖĞRETİM KURULU
DOKÜMANTASYON MERKEZİ**

**by
Aytaç Gürhan GÖKÇE**

119572

**July, 2002
İZMİR**

119572

ACKNOWLEDGEMENTS

I would like to express my deepest gratitude to my supervisor Assistant Prof. Muhittin AYGÜN for his continual presence, invaluable guidance and endless patience throughout the course of this work.

I am greatly indebted to Nilgün AKKUŞ and Prof. Dr. Bekir ÇETİNKAYA for their help.

I also would like to thank to Ümit AKINCI and Hakan AKMAZ for their technical supports and close friendships.

Finally, my deepest gratitude goes to my family and Melis KOÇAN whose constant support, patience made me keep going.


Aytaç Gürhan GÖKÇE

Ms.Sc. THESIS EXAMINATION RESULT FORM

We certify that we have read the thesis, entitled “**THE CRYSTAL STRUCTURE ANALYSIS OF $C_{24}H_{28}N_2O_4$ AND $C_{23}H_{32}N_4SE$ BY SINGLE CRYSTAL X-RAY DIFFRACTION TECHNIQUE**” completed by **Aytaç Gürhan GÖKÇE** under supervision of **Yard. Doç. Dr. Muhittin AYGÜN** and that in our opinion it is fully adequate, in scope and in quality, as a thesis for the degree of Master of Science.


Yard. Doç. Dr. Muhittin AYGÜN

Supervisor


Prof. Dr. Mustafa EROL

Committee Member


Prof. Dr. Bünyamin ÖZBAY

Committee Member

Approved by the
Graduate School of Natural and Applied Sciences


Prof. Dr. Cahit Helvacı

Director

ABSTRACT

Molecular and crystal structures of '3,3'-dimethoxybenzidine(2-hydroxybenzal) diimine' and 'hexahydrobis[(1,3-*p*-dimethylamino-benzyl)-1,3-diazepine-2-selenone] have been determined by single crystal X-ray diffraction study.

The crystal structure of $C_{28}H_{24}N_2O_4$ was solved by direct methods with using a total of 2325 reflections for $I)2\sigma(I)$. Structure was refined by full-matrix least-square and difference-Fourier methods to a conventional R value of 0.056 for 203 parameters. There is half independent molecule in the asymmetric unit and molecular structure is formed with $(-x, y, -z - \frac{1}{2})$ symmetry operator. The molecule has a two-fold symmetry on the mid point of the C4-C4' bond. The N1=C8 imine bond length of 1.284(3) Å is typical of a double bond. There is imine moiety, hydroxyphenyl ring and methoxyphenyl ring planes in the molecule and the molecule of the title compound is not planar. There is a strong intramolecular hydrogen bond between hydroxy oxygen atom and imine nitrogen atom. The crystal structure is stabilized by one weak intermolecular hydrogen bond of the C-H...O type and also by van der Waals interactions. Crystallographic data for $C_{28}H_{24}N_2O_4$: Monoclinic, C2/c, $a = 18.045(2)$ Å, $b = 11.725(4)$ Å, $c = 12.436(6)$ Å, $\beta = 120.03(3)^\circ$, $Z = 4$, $D_x = 1.32$ g/cm³, $\mu(MoK_\alpha) = 0.089$ mm⁻¹, $V = 2278.0(14)$ Å³, $F_{000} = 952$, $R_1 = 0.056$, $wR_2 = 0.167$, $GOF = 1.088$, $\Delta\rho_{\min} = -0.202$, $\Delta\rho_{\max} = 0.180$, $(\Delta/\sigma)_{\max} = 0.003$.

The crystal structure of $C_{23}H_{32}N_4Se$ was solved by direct methods. Using full-matrix least-square and difference-Fourier methods, the 291 atomic parameters were refined to a final $R = 0.061$ for 2626 reflections with $I > 2\sigma(I)$. The non-hydrogen atoms were refined anisotropically. The diazepine ring proved to be disordered over two orientations. The four C atoms except C1 in diazepine ring have site-occupation factor values of nearly 0.53(1) and 0.47(1). The Se=C bond length of 1.862(5)Å is typical of a double bond. The displacement parameters of disordered C atoms of the diazepine ring are quite high, resulting in unusual bond lengths involving these atoms. The dihedral angle between the two phenyl rings is 37.7(2)°. The two dimethylamino group is planar. There are three intramolecular interactions: two of them are C-H...Se type and the other one is C-H...N type. The molecules in the crystal are packed by normal van der Waals distances. Crystallographic data for

$C_{23}H_{32}N_4Se$: Orthorhombic, Pbc_a, $a = 10.996(1)$ Å, $b = 14.946(1)$ Å,
 $c = 27.565(5)$ Å, $Z = 8$, $D_x = 1.30$ g/cm³, $\mu(MoK_\alpha) = 1.673$ mm⁻¹,
 $V = 4530.2(9)$ Å³, $F_{000} = 1856$, $R_1 = 0.061$, $wR_2 = 0.180$, GOF = 1.070,
 $\Delta\rho_{\min} = -0.548$, $\Delta\rho_{\max} = 0.492$, $(\Delta/\sigma)_{\max} = 0.005$.

ÖZET

‘3,3’-dimetoksibenzidin(2-hidroksibenzal)diimin’ ve ‘heksahidrobis[(1,3-*p*-dimetilamino-benzil)-1,3-diazepin-2-selenon’ moleküllerinin moleküler ve kristal yapıları tek kristal x-ışını kırınımı yöntemiyle çözülmüştür.

$C_{28}H_{24}N_2O_4$ molekülünün kristal yapısı $I)2\sigma(I)$ koşulunu sağlayan 2325 yansıma kullanılarak, direk yöntemlerle çözülmüştür. Tam-matris en.küçük kareler ve fark-Fourier yöntemleri kullanılarak 203 atomik parametrenin artırılması sonucu $R = 0.056$ değerine ulaşılmıştır. Asimetrik birimde molekülün yarısı bulunmaktadır ve $(-x, y, -z - \frac{1}{2})$ simetri işlemiyle moleküler yapı tamamlanmaktadır. Molekül $C_4 - C_4'$ bağının orta noktasında 2-dönerli simetri eksenine sahiptir. $N_1=C_8$ bağının uzunluğu $1.284(3) \text{ \AA}$ olup, tipik çift bağ özelliği göstermektedir. Molekülde imin kısmı, hidroksifenil halkası ve metoksifenil halkası düzlemleri olup, molekülün düzlemsel olmadığı saptanmıştır. İmin kısmındaki azot atomu ile hidroksi kısmındaki oksijen atomu arasında molekül içi güçlü bir hidrojen bağı vardır. Kristal yapı moleküller arası C-H...O tipi zayıf bir hidrojen bağı ve van der Waals etkileşimleriyle kararlı durumdadır. $C_{28}H_{24}N_2O_4$ molekülü için kristalografik veriler: Monoklinik, $C2/c$, $a = 18.045(2) \text{ \AA}$, $b = 11.725(4) \text{ \AA}$, $c = 12.436(6) \text{ \AA}$, $\beta = 120.03(3)^\circ$, $Z = 4$, $D_x = 1.32 \text{ g/cm}^3$, $\mu(MoK_\alpha) = 0.089 \text{ mm}^{-1}$, $V = 2278.0(14) \text{ \AA}^3$, $F_{000} = 952$, $R_I = 0.056$, $wR_2 = 0.167$, $GOF = 1.088$, $\Delta\rho_{\min} = -0.202$, $\Delta\rho_{\max} = 0.180$, $(\Delta/\sigma)_{\max} = 0.003$.

$C_{23}H_{32}N_4Se$ molekülünün kristal yapısı direk yöntemlerle çözülmüştür. Tam-matris en küçük kareler ve fark-Fourier yöntemleri kullanılarak, 291 atomik parametre, $I > 2\sigma(I)$ koşulunu sağlayan 2626 yansıma için $R = 0.061$ değerine artırılmıştır. Hidrojen atomları hariç tüm atomlar anizotropik olarak artırılmıştır. Diazepin halkasının disorder'lı olduğu ve iki kısma ayrıldığı görülmüştür. Bu halkada C1 hariç diğer dört C atomunun 'sof' değerleri yaklaşık olarak 0.53(1) ve 0.47(1)'dir. Se=C bağının uzunluğu 1.862(5) Å olup, tipik çift bağ özelliği göstermektedir. Diazepin halkasındaki disorder'lı C atomlarının yerdeğiştirme parametreleri oldukça yüksektir, buna bağlı olarak bu atomlar arasında anormal bağ uzunlukları ortaya çıkmıştır. İki fenil halkası arasındaki dihedral açının $37.7(2)^\circ$ olduğu saptanmıştır. İki dimetilamino grubu da düzlemseldir. Molekülde üç molekül içi etkileşim vardır: bunlardan ikisi C-H...Se tipi ve diğeri ise C-H...N tipidir. Kristaldeki moleküller normal van der Waals uzaklıkları ile yerleşmişlerdir. $C_{23}H_{32}N_4Se$ molekülü için kristalografik veriler: Ortorombik, Pbc_a, $a = 10.996(1)\text{Å}$, $b = 14.946(1)\text{Å}$, $c = 27.565(5)\text{Å}$, $Z = 8$, $D_x = 1.30\text{ g/cm}^3$, $\mu(\text{MoK}_\alpha) = 1.673\text{ mm}^{-1}$, $V = 4530.2(9)\text{ Å}^3$, $F_{000} = 1856$, $R_1 = 0.061$, $wR_2 = 0.180$, $\text{GOF} = 1.070$, $\Delta\rho_{\min} = -0.548$, $\Delta\rho_{\max} = 0.492$, $(\Delta/\sigma)_{\max} = 0.005$.

CONTENTS

	Page
Contents.....	ix
List of Figures.....	xiii
List of Tables.....	xv
Symbols.....	xvii

Chapter One INTRODUCTION

1.1 Introduction.....	1
-----------------------	---

Chapter Two X-RAYS

2.1 The Discovery of X-Rays.....	4
2.2 X-Ray Tube.....	5
2.3 The Wave Nature of X-Rays.....	6
2.4 Generation of X-Rays.....	7
2.5 X-Ray Sources.....	10

Chapter Three

X-RAY DIFFRACTION DATA

3.1 The Geometry of Enraf-Nonius CAD-4 Diffractometer	12
3.2 Bragg's Law.....	15
3.3 Measurement Methods of Diffraction Intensities.....	16
3.4 Scattering of X-Rays by a Crystal.....	17
3.5 Crystal Structure Factor.....	19
3.6 Fourier Synthesis and Electron Density.....	20
3.7 The Phase Problem.....	21
3.8 Data Reduction.....	23
3.8.1 Lorentz Correction.....	24
3.8.2 Polarization Correction.....	24
3.8.3 Absorption Correction.....	24
3.8.4 Debye-Waller Temperature Factor Correction.....	26
3.8.5 Extinction Correction.....	28
3.8.6 Anomalous Scattering Factor.....	29

Chapter Four

SOLUTION OF CRYSTAL STRUCTURE

4.1 Introduction.....	30
4.1.1 The trial-and-error method.....	30
4.1.2 The Patterson Technique.....	31
4.2 Direct Methods.....	31
4.2.1 Background and Early History.....	31
4.2.2 Normalized Structure Factors and Intensity Statistics.....	33
4.2.3 Centrosymmetric Structures.....	34
4.2.4 Non-centrosymmetric Structures.....	35
4.2.5 Criteria of Correctness Set of Phases.....	36
4.2.5.1 MABS.....	36
4.2.5.2 NQUAL.....	37
4.2.5.3 R_{α} FOM.....	37

Chapter Five

CRYSTAL STRUCTURE REFINEMENT

5.1 Refinement Methods.....	38
5.1.1 Difference Fourier Method.....	38
5.1.2 Least-Squares Method.....	39
5.1.2.1 Overall Strategy.....	40
5.2 Error Analysis.....	41
5.2.1 R Factors.....	41
5.2.2 Goodness of Fit.....	41
5.2.3 Final Difference Map.....	42
5.2.4 Estimated Standard Deviations.....	42

Chapter Six

EXPERIMENTAL DETAILS

6.1 The Crystal of $C_{28}H_{24}N_2O_4$	43
6.1.1 Synthesis of $C_{28}H_{24}N_2O_4$ Crystal.....	43
6.1.2 Data Collection of $C_{28}H_{24}N_2O_4$ Crystal.....	44
6.1.3 Structure Solution&Refinement of $C_{28}H_{24}N_2O_4$ Crystal.....	45
6.1.4 Experimental Results for $C_{28}H_{24}N_2O_4$ Crystal.....	45
6.1.5 Molecular Graphics of $C_{28}H_{24}N_2O_4$ Crystal.....	53
6.2 The Crystal of $C_{23}H_{32}N_4Se$	58
6.2.1 Synthesis of $C_{23}H_{32}N_4Se$ Crystal.....	58
6.2.2 Data Collection of $C_{23}H_{32}N_4Se$ Crystal.....	59
6.2.3 Structure Solution&Refinement of $C_{23}H_{32}N_4Se$ Crystal.....	60
6.2.4 Experimental Results for $C_{23}H_{32}N_4Se$ Crystal.....	60
6.2.5 Molecular Graphics of $C_{23}H_{32}N_4Se$ Crystal.....	70

Chapter Seven
CONCLUSION

7.1 Conclusion.....74

References.....77



LIST OF FIGURES

	Page
Figure 1.1 The chemical diagram of “3,3’-dimethoxybenzidine(2-hydroxybenzal)diimine” crystal.....	1
Figure 1.2 The chemical diagram of “hexahydrobis[(1,3- <i>p</i> -dimethylamino-benzyl)-1,3-diazepine-2-selenone”.....	2
Figure 2.1 The electromagnetic spectrum	4
Figure 2.2 Schematic of an x-ray tube	6
Figure 2.3 A plot of the bremsstrahlung intensity as a function of increasing accelerating voltage	8
Figure 2.4 X-Ray spectra for Cu and Mo targets showing the characteristic lines	8
Figure 2.5 A diagram of the energy transitions that give rise to the characteristic lines	9
Figure 2.6 Schema of sealed tube generator	11
Figure 2.7 Schema of rotating anode generator	11
Figure 3.1 The κ geometry goniometer.....	13
Figure 3.2 The geometry of the CAD-4 diffractometer.....	14
Figure 3.3 Arrangement of the sodium and chloride ions in a rock salt crystal	16
Figure 3.4 Derivation of Bragg’s formula.....	16
Figure 3.5 Diffractometer scan types. (a) w -scan (b) $w/2\theta$ -scan.....	17
Figure 3.6 Combination of N waves on an Argand diagram.....	18
Figure 3.7 Atomic scattering factors: (a) stationary atom, (b) atom corrected for thermal vibration.....	20

Figure 3.8	Wilson plot.....	28
Figure 3.9	Anomalous scattering of atom A with respect to the rest of the structure R: (a) normal case- $ F(h) = F(\bar{h}) $; (b) anomalous case- $ F(h) \neq F(\bar{h}) $	29
Figure 6.1	Synthetic route for the preparation of “3,3’-dimethoxybenzidine (2-hydroxybenzal)diimine”	43
Figure 6.2	There is half-independent molecule in the asymmetric unit.....	54
Figure 6.3	An ORTEP3 drawing of $C_{28}H_{24}N_2O_4$ showing the atomic numbering scheme.....	55
Figure 6.4	Unit cell contents with the hydrogen-bonding scheme indicated by dashed lines. [symmetry code: (ii) $\frac{1}{2}-x, \frac{1}{2}+y, \frac{1}{2}-z$]	56
Figure 6.5	A CPK drawing of $C_{28}H_{24}N_2O_4$	57
Figure 6.6	The chemical reaction of $C_{23}H_{32}N_4Se$	58
Figure 6.7	An ORTEP3 view of the $C_{23}H_{32}N_4Se$ with the non-H atoms shown with displacement ellipsoids drawn at the 30% probability level.....	71
Figure 6.8	Unit cell packing diagram of $C_{23}H_{32}N_4Se$	72
Figure 6.9	A CPK drawing of the $C_{23}H_{32}N_4Se$	73

LIST OF TABLES

		Page
Table 2.1	Target materials and associated constants.....	10
Table 3.1	Atomic mass and mass absorption coefficients for $C_{28}H_{24}N_2O_4$	25
Table 3.2	Atomic mass and mass absorption coefficients for $C_{23}H_{32}N_4Se$	25
Table 4.1	Some statistical properties of normalized structure factor magnitudes.....	34
Table 6.1	FOM values for $C_{28}H_{24}N_2O_4$	45
Table 6.2	Crystallographic data for for $C_{28}H_{24}N_2O_4$	45
Table 6.3	Atomic coordinates and equivalent isotropic thermal parameters.....	47
Table 6.4	Anisotropic displacement parameters.....	48
Table 6.5	Bond Distances.....	49
Table 6.6	Bond Angles.....	50
Table 6.7	Torsion Angles.....	51
Table 6.8	Hydrogen Bonds.....	52
Table 6.9	Standard deviations of atoms from the planes.....	52
Table 6.10	Dihedral Angles.....	53
Table 6.11	FOM values for $C_{23}H_{32}N_4Se$	60
Table 6.12	Crystallographic data for $C_{23}H_{32}N_4Se$	60
Table 6.13	Atomic coordinates and equivalent isotropic thermal parameters.....	62
Table 6.14	Anisotropic displacement parameters.....	65
Table 6.15	Bond distances.....	66
Table 6.16	Bond angles.....	67

Table 6.17	Torsion angles.....	68
Table 6.18	Standard deviations of atoms from the planes.....	70
Table 6.19	Dihedral angles.....	70



CHAPTER ONE

INTRODUCTION

1.1 Introduction

In this research, the crystal structures of “3,3’-dimethoxybenzidine(2-hydroxybenzal)diimine”, ($C_{28}H_{24}N_2O_4$), which is one of the Schiff base compounds, and ‘hexahydrobis[(1,3-*p*-dimethylamino-benzyl)-1,3-diazepine-2-selenone’, ($C_{23}H_{32}N_4Se$), is determined by single crystal X-ray diffraction technique. The chemical diagrams of these compounds are given in Figure 1.1 and Figure 1.2, respectively.

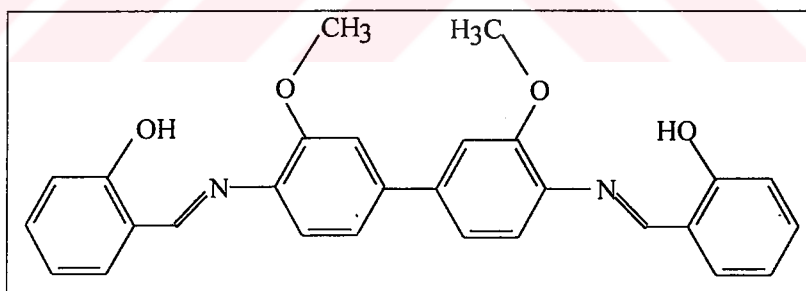


Figure 1.1 The chemical diagram of “3,3’-dimethoxybenzidine (2-hydroxybenzal)diimine”.

Interest in imine derivatives has increased greatly during recent years due to their different applications in various areas. The formation of Schiff bases may proceed readily in many cases under relatively mild conditions. It is therefore not surprising that biochemistry, biomedical research, immunochemistry *etc.* have found uses for

the reaction of amines (Sandler&Karo, 1986; Chen&Rhodes, 1996). Most Schiff bases possess antibacterial, anticancer, and antitoxic activities (Williams, 1972).

There has been considerable interest in some Schiff bases derived from salicylaldehyde because they show thermochromism and photochromism in the solid state. This behavior may involve reversible proton transfer from the hydroxyl-O atom to the imine-N atom (Cohen et al., 1964; Hadjoudis et al., 1987). Photochromism and thermochromism are produced by the intramolecular proton transfer associated with a change in π – electron configuration (Barbara et al., 1980; Hadjoudis, 1981). Photochromic compounds are of great interest because of their application area in constructing the optical switches or optical memory devices (Schmidt, 1976). The title compound shows photochromism. It has been proposed that molecules showing thermochromism are planar, while those showing photochromism are non-planar, both phenomena being associated with a proton transfer. Consequently, it is evident that a closely related phenomenon of interest is the possibility of tautomeric isomerism in ortho-hydroxy Schiff bases (Fernandez et al., 2001; Hadjoudis et al., 1987).

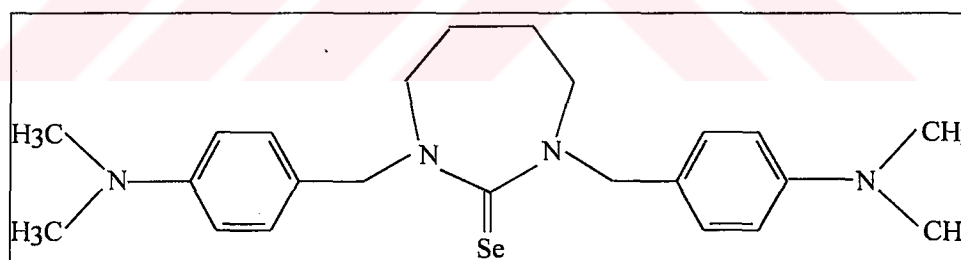


Figure 1.2 The chemical diagram of “hexahydrobis[(1,3-*p*-dimethylamino-benzyl)-1,3-diazepine-2-selenone”.

The determined “hexahydrobis[(1,3-*p*-dimethylamino-benzyl)-1,3-diazepine-2-selenone” hasn’t been studied extensively although the diazepine ring in the molecule and its derivatives have been investigated widely in many studies (Insuasty et al., 2001; Martinez et al., 1996; Cogordan et al., 1998). The most known derivatives of the diazepine are benzodiazepine and oxadiazepine. Benzodiazepines

earned a lot of popularity because of high therapeutic index and diazepam molecule apparently has structural resemblance to benzodiazepam molecule (Wafai&Mehta, 1986). 1,4-benzodiazepines have been the object of intense studies since the early 1960s because of their value in psychotherapy (Sabatie et al., 2001). The synthesis of the oxadiazepam was reported while the investigation of the chemotherapeutic use of a series of heterocycles (Ochoa et al., 2001).

In our study, X-ray data for the crystal structures are collected with Enraf Nonius CAD-4 diffractometer that is at X-Ray Laboratory, Department of Physics Engineering, Faculty of Engineering, Hacettepe University. After this, the collected data are solved by direct methods with SHELXS-97 (Sheldrick, 1998) program and the atomic parameters are refined by least squares and difference-Fourier method with SHELXL-97 (Sheldrick, 1998) program at Department of Physics, Faculty of Arts&Sciences, Dokuz Eylül University. In different steps of the study for geometrical calculations and molecular graphics; WINGX (Farrugia, 1999), ORTEP3 (Farrugia, 1997), PLATON (Spek, 1990), PLUTON (Spek, 1990) package programs were used. Also the chemical diagrams were formed by CHEMWIN program.

CHAPTER TWO

X-RAYS

W. K. Roentgen, who assigned this name because the true nature of the radiation was at first unknown, discovered X-rays, also called Roentgen rays, in 1895. Today we know that Roentgen's X-rays are electromagnetic radiation with short wavelengths λ ranging from 0.1\AA to 100\AA that is shown in Figure 2.1. X-rays shorter than 1\AA are usually called hard X-rays while those longer than 1\AA are known as soft X-rays.

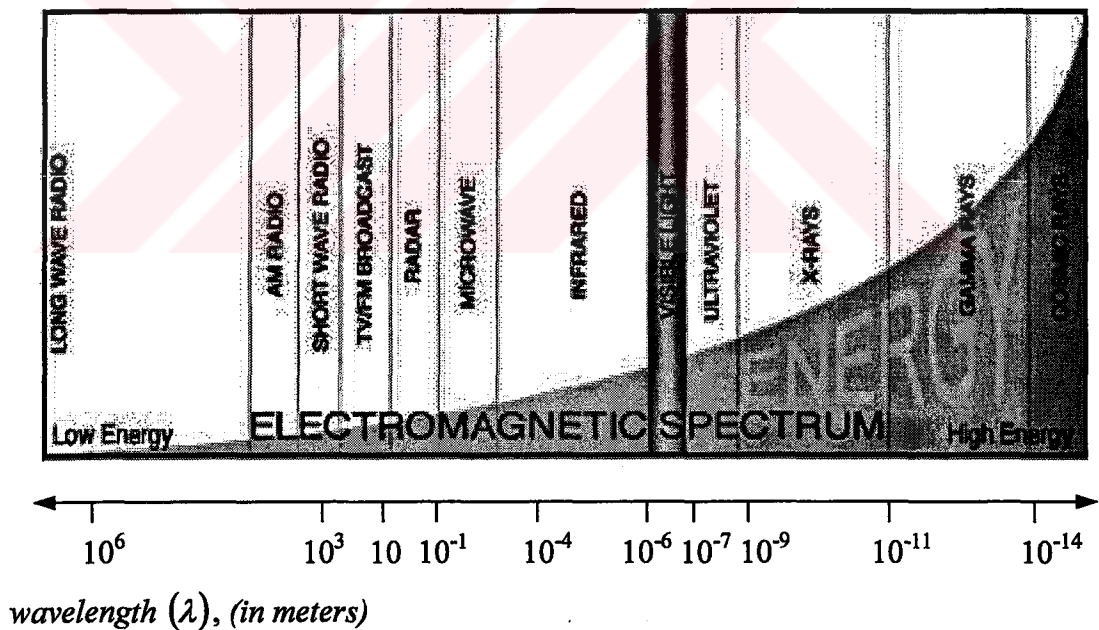


Figure 2.1 The electromagnetic spectrum.

2.1 The Discovery of X-Rays

In 1895, Roentgen performed an experiment on a gas discharge in a cathode ray tube in a darkroom. The cathode ray tube is also called the Crookes tube after the

British physicist W. Crookes who developed it. Roentgen wrapped a cathode ray tube with black paper purposely to avoid the influence of ultraviolet and visible light. He found that a fluorescent screen treated with barium platinum cyanide, $\text{BaPt}(\text{CN})_6$ at some distances from the tube still exhibited slight fluorescence. Through repeated experiments, he made sure that the cause of the activation of the fluorescence came from the cathode ray tube, but that it was by no means the cathode rays themselves.

Over the next month or more, Roentgen made several kinds of studies on this mysterious new ray that produced the fluorescence. He found that these rays traveled straight, were not deflected by a magnetic field, and could go about 2m in air. Soon he discovered the penetrating power of the rays, which allowed photographs of the outline of a balance scale and other objects put in a closed box to be taken. Considering the mystery and the uncertainty of the rays he had discovered, he named them X-rays. Roentgen read his first report "On the New Ray" at the end of 1895 and published a radiograph of the finger bone of his wife. Roentgen's discovery resulted in extremely rapid responses all over the world. Astonishingly, in 1896 there were about one thousand papers published on studies of X-rays or their application. This is truly remarkable because this was before our time when so much emphasis is placed on publication (Yang&Hamilton, 1996).

Following the discovery of X-rays, a new period of physics began. Together with the discoveries of radioactivity and the electron in the next two years, it opened up the world of modern physics. Before these discoveries scientists thought that all the basic principles of physics were known.

2.2 X-Ray Tube

There are various ways to construct tubes to produce X-rays. Figure 2.2 is a general representation of an X-ray tube that used by Roentgen. With a pressure $10^{-6} - 10^{-8} \text{ mmHg}$, electrons from the heated cathode K are accelerated easily by the electric field to the anode A. The X-rays are produced when the electrons strike the anode. The anode is typically made of a heavy metal such as tungsten, molybdenum

or platinum. In 1895, the electrical potential difference used by Roentgen was only several thousand volts, so the energy of the electrons was comparatively low and the rays produced were soft X-rays. Today accelerating voltage between the cathode and the anode is generally $10^4 V$ to $10^5 V$. Changing this voltage changes the energy of the electrons that strike the anode and so changes the X-ray energy (frequency).

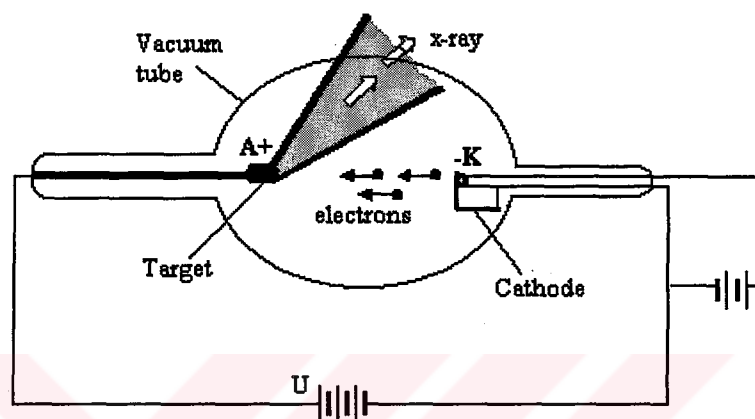


Figure 2.2 Schematic of an X-ray tube.

When deciding which type of X-ray tube to use, the practical crystallographer must be aware of three features. The first is the choice of targets material and the radiation filter. Tubes with *Cr*, *Fe*, *Cu*, *Mo* and *Ag* targets are commercially available. The second and the third important properties of an X-ray tube are the sizes of the focal point and the power, since the X-ray intensity depends on these parameters.

2.3 The Wave Nature of X-Rays

J. C. Maxwell concluded that an accelerated charged particle can radiate an electromagnetic wave. Thus, when a target stops high-speed electrons, they produce electromagnetic waves, and it would seem logical to think of X-rays as electromagnetic waves. But Roentgen didn't observe X-ray refraction, reflection or diffraction. He therefore thought, incorrectly, that X-rays were not a form of electromagnetic radiation. In 1906, C. G. Barkla was confirmed the wave nature of X-rays for the first time experimentally by demonstrating the polarization of X-rays.

But M. von Laue, who proposed a method for measuring the wavelengths of X-rays, supplied the conclusive proof of the wave nature of X-rays in 1912. It occurred to Laue that the separations between the atoms in a crystal might be of the same order of magnitude as the wavelengths of the X-rays. If so, X-rays passing through a crystal exhibit distinctive interference effects, like the other interference effects of light passing through a grating. W. Friedrich and P. Knipping performed the experiment.

2.4 Generation of X-Rays

As Roentgen demonstrated X-rays are produced when electrons of high speed hit a target metal and are rapidly decelerated. Since this deceleration process usually involves multiple collisions a continuum of radiation (Figure 2.3) is formed. This continuous spectrum is called "white radiation" or "bremsstrahlung" (braking radiation). It is evident from Figure 2.3 that the wavelength range of the bremsstrahlung is dependent only on the accelerating voltage (V_{acc}) and that each voltage has a characteristic minimum wavelength (λ_{min}), which can be calculated by the following equation

$$eV = \frac{hc}{\lambda_{min}} \Rightarrow \lambda_{min} = \frac{hc}{eV} \quad (2.1)$$

Taking the numerical values for the constants, (h, c, e);

$$\lambda_{min} = \frac{12398}{V_{acc}} \quad (2.2)$$

This equation is known as the Duane-Hunt law and predicts that λ_{min} will shift towards shorter wavelengths (higher energy) as the accelerating voltage is increased. For a fixed voltage the maximum intensity is at a λ - value of about 1.5 times λ_{min} .

When the energy of the electrons striking the target is higher than a certain threshold value, a second type of spectrum, discontinuum and with very sharp lines, appears superimposed on the white radiation curves just described. This second radiation is called "characteristic radiation" because its peaks are found at precisely

defined wavelengths, which depend on the material constituting the target. The characteristic spectrum of Copper and Molybdenum is shown in Figure 2.4.

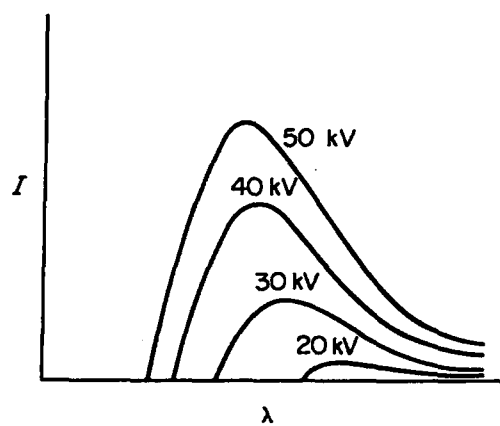


Figure 2.3 A plot of the bremsstrahlung intensity as a function of increasing accelerating voltage.

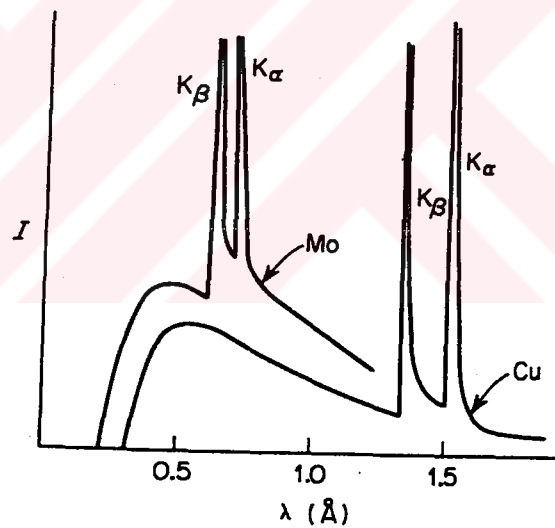


Figure 2.4 X-Ray spectra for Cu and Mo target showing the characteristic lines.

A 10000 eV potential is sufficient to remove an electron from the K shell for Cu. An electron from the outer shells immediately fills this vacancy in the K shell. The energy released during the transition is in the form of nearly monochromatic X-rays. Thus, the characteristic lines represent the L→K, M→K and M→L electron transitions (Figure 2.5), which are unique for each element. Only the L→K and M→K transitions are important for X-ray diffraction studies.

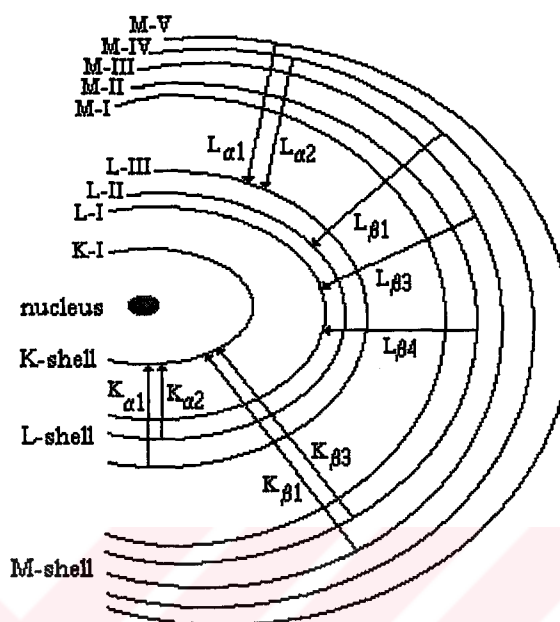


Figure 2.5 A diagram of the energy transitions that give rise to the characteristic lines.

The frequency of the characteristic line corresponding to a given transition is related to the atomic number of the element that gave rise to it, Z , by Moseley's law

$$\frac{1}{\lambda} = p(Z - \sigma)^2 \quad (2.3)$$

where p is a constant related to the principle quantum numbers of the shells and σ is a screening constant that accounts the interactions with other electrons.

The characteristic wavelengths for some elements commonly used in commercial X-ray tubes are listed in Table 2.1. The elements, used for X-ray structure determinations, are Copper and Molybdenum. Copper is the choice for organic and protein crystals and Molybdenum used for inorganic crystals because of severe absorption.

Table 2.1 Target materials and associated constants

	Cr	Fe	Cu	Mo
Z	24	26	29	42
α_1 (Å)	2.2896	1.9360	1.5404	0.70926
α_2 (Å)	2.2935	1.9399	1.5443	0.71354
$\langle\alpha\rangle$ (Å)	2.2909	1.9373	1.5418	0.71069
β_1 (Å)	2.0848	1.7565	1.3922	0.63225
β filter	V	Mn	Ni	Nb
(Å)	0.01 mm	0.01 mm	0.015 mm	0.075 mm

2.5 X-Ray Sources

As stated previously, bombarding a metal target with high-energy electrons can produce X-rays. This is the conventional method used to produce laboratory X-rays. Another method of producing X-rays is synchrotron storage rings.

The two most common types of X-rays generators in use today are the sealed tube generator (Figure 2.6) and the rotating anode generator (Figure 2.7). In both generators, electrons are boiled off a tungsten filament (cathode) by the application of an electrical current. The electrons are then accelerated towards the target (anode) by applying a large potential difference (40-50 kV) between the anode and the cathode.

In the sealed tube generators, X-rays are produced in a permanently sealed X-ray tube, and heat is removed by a water-cooled heat sink to which the target is attached.

Thus, although simple and easy to maintain, the sealed tube design is limited by the amount of heat and that can be removed from the target, this restricts the operating range to between 1 to 2 kW . Rotating anode X-ray generators were developed to increase the efficiency of heat transfer from the target by providing a

larger area for electron impact. In the rotating anode generator, a rotating cylindrically shaped water-cooled target (anode) allows the heat generated by electron impact to be spread over a large area. This allows the rotating anode generator to be operated at power levels ranging from 3 to 18 kW . The rotating anode generator is mechanically more complicated than the sealed tube generator since it requires a high vacuum system and special seals to maintain the vacuum (Lecture Notes, 2001).

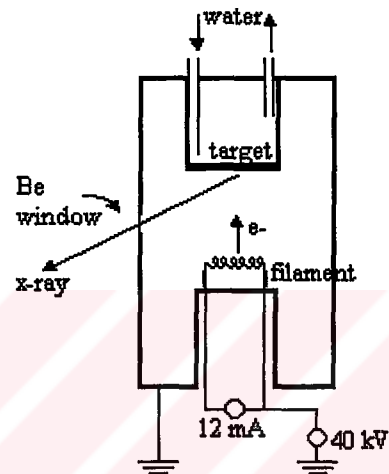


Figure 2.6 Schema of sealed tube generator.

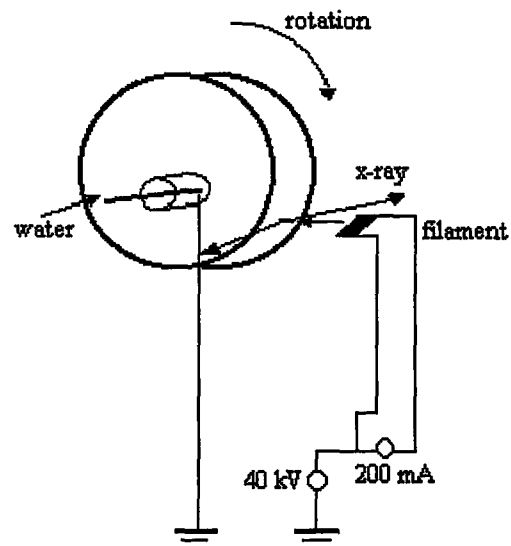


Figure 2.7 Schema of rotating anode generator

CHAPTER THREE

X-RAY DIFFRACTION DATA

X-rays that scattered by single crystals, diffracted belong to Bragg's law. The intensities and the orientations of the diffracted X-rays, depend on the atoms positions and the number of electrons in the unit cell. By evaluation of intensity data the structure of molecules can be explained. In other words, unit cell parameters (crystal system, space group, $a, b, c, \alpha, \beta, \gamma$), atom positions, bond distances, bond angles, torsion angles and atomic displacement parameters which belongs to the crystal structure can be determined.

Before the determination of crystal structures, geometry of diffractometer, which is used to collect the data, must be investigate.

3.1 The Geometry of Enraf-Nonius CAD-4 Diffractometer

In this study, the data were collected with an Enraf-Nonius CAD-4 diffractometer. "A single crystal diffractometer consist of an X-ray source, an X-ray detector, a goniometer that orients the crystal so that a chosen X-ray diffracted beam can be received by the detector, and a computer that controls the goniometer and detector movements and performs the mathematical operations required to position the crystal and the detector in the desired orientations" (Giacovazzo, 1998, p.273).

In all single crystal diffractometers, the detector defines a plane that contains the incident and the diffracted beams. But the geometry of the CAD-4 (Kappa Axis

Diffractometer) diffractometer is different from the geometry of four circle diffractometers.

The following discussion refers to Figure 3.2. The goniometer head has three manual translational adjustments called x , y and z , which are used to position the center of the sample crystal in the center of the goniometer. The goniometer head carrying the crystal is mounted on an arm that can rotate about an axis, κ - axis . The κ geometry of the goniometer is shown in Figure 3.1. κ - axis passes through the center of the goniometer and makes the angle of 50° to the Φ - axis and to the w - axis . Both, the Φ - axis and the w - axis pass through the center of the goniometer.

With this arrangement, it is possible to move any vector whose base is at the center of the crystal to any position. It is also possible to rotate the crystal with a combination of Φ -, κ - and w - rotations.

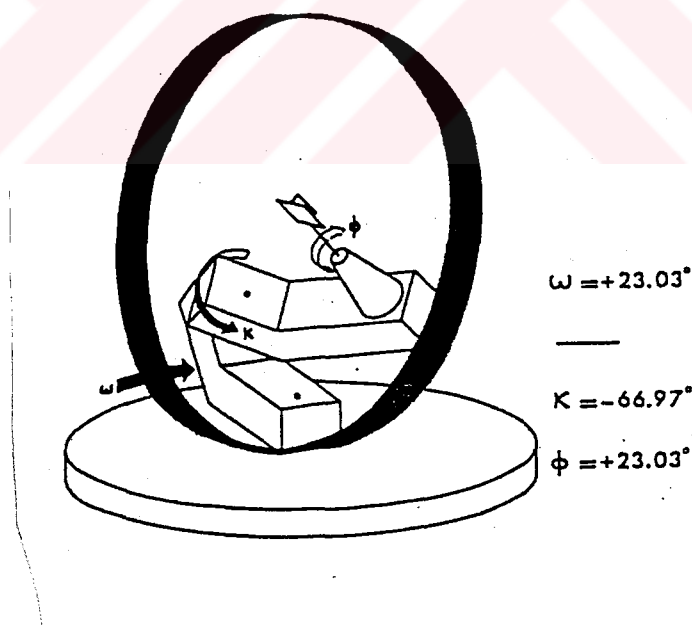


Figure 3.1 The κ geometry goniometer.

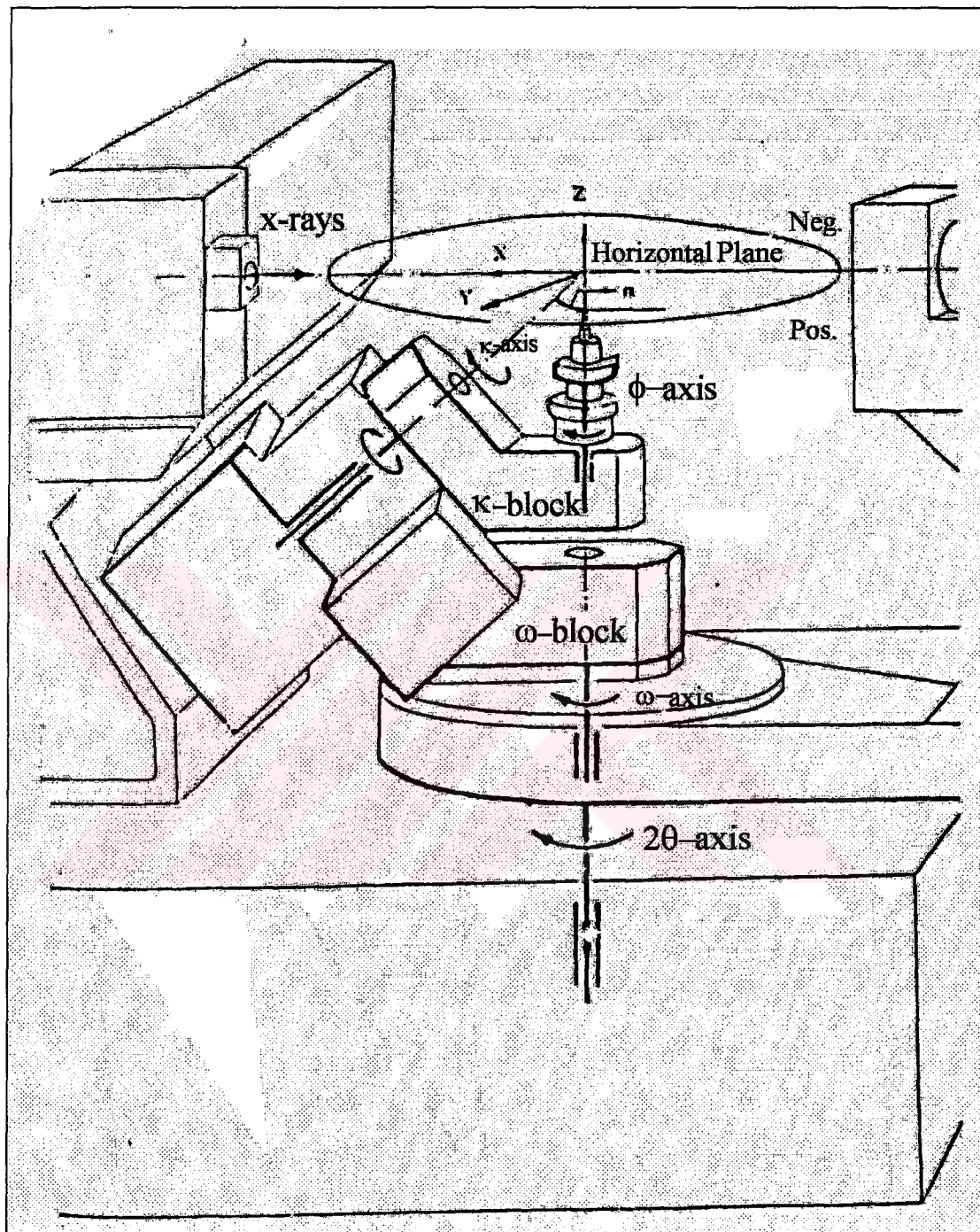


Figure 3.2 The geometry of the CAD-4 diffractometer.

3.2 Bragg's Law

Since X-rays have wavelengths the order of an angstrom, it is rather difficult to make a slit of this size to observe diffraction of X-rays. Von Laue first suggested the use of the planes of atoms in a crystal as the natural grating (set of slits) to observe the diffraction of X-rays. Figure 3.3 shows the arrangement of the chlorine ions and sodium ions in a rock salt crystal. We will see that the spacing of atoms in the planes of such a crystal grating are of the same order as X-rays wavelengths. But first look at what happens when X-rays strike crystal lattices.

As shown in Figure 3.4, an incident X-ray makes an angle θ with the crystal plane. If this crystal plane is a mirror plane, it is easy to show that the path difference between ray1 and ray2, $AC + CD$, is equal to $2d \sin \theta$. When it is an integral multiple n of the wavelength, we have

$$2d \sin \theta = n\lambda \quad n = 1, 2, \dots \quad (3.1)$$

where d is the lattice spacing, λ is the incident X-ray wavelength and θ is the incident and reflected angle. The X-rays reflected in the direction θ will have a maximum in their diffraction intensity. (3.1) is called the Bragg Law. When a beam of X-rays strikes a crystal, it must satisfy the Bragg Law for its reflected rays to be intensified by diffraction. From this equation we know that the wavelength must be smaller than $2d$, and, if either λ or d is known, the other can be calculated after measuring θ in a diffraction experiment (Yang&Hamilton, 1996).

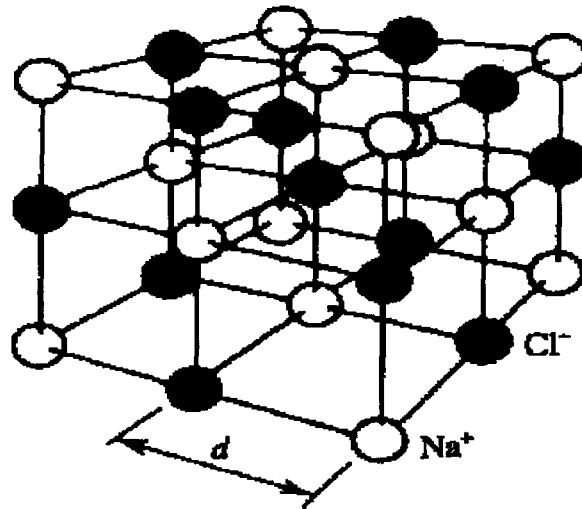


Figure 3.3 Arrangement of the sodium and chloride ions in a rock salt crystal.

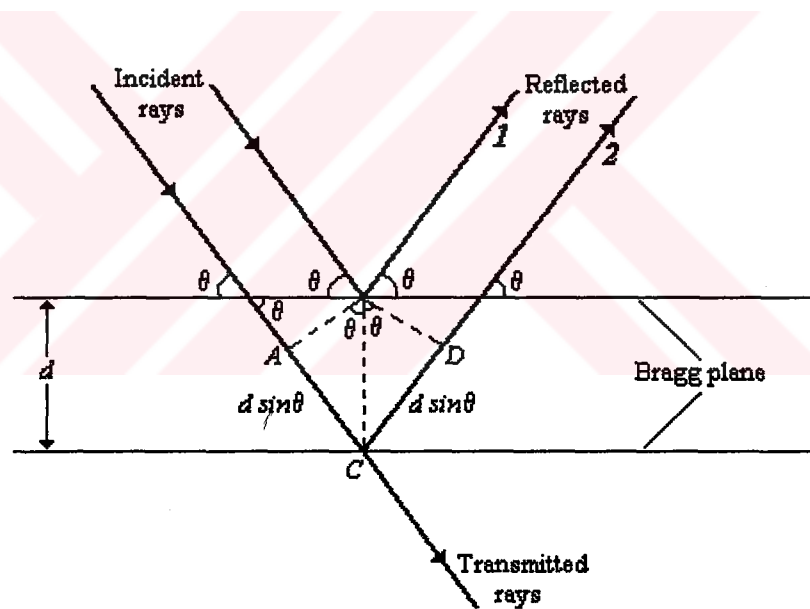


Figure 3.4 Derivation of Bragg's formula.

3.3 Measurement Methods of Diffraction Intensities

There are three well-known methods for measurement of diffraction intensities. In first of these, both crystal and detector are not moved. While crystal is constant at the reflection position, detector is constant at the 2θ position and intensity measured.

In the “ w -scan” mode, the detector is held at the 2θ angle of the actual reflection and the crystal rotated on the w -axis of the diffractometer.

In the “ $w/2\theta$ -scan” mode, both crystal and detector are moved. The crystal is rotated by Δw , while the detector is rotated in the 2θ -circle by an angular velocity, which is twice of the crystal rotation.

The principles of “ w -scan” and “ $w/2\theta$ -scan” methods are shown in Figure 3.5(a) and 3.5(b), respectively.

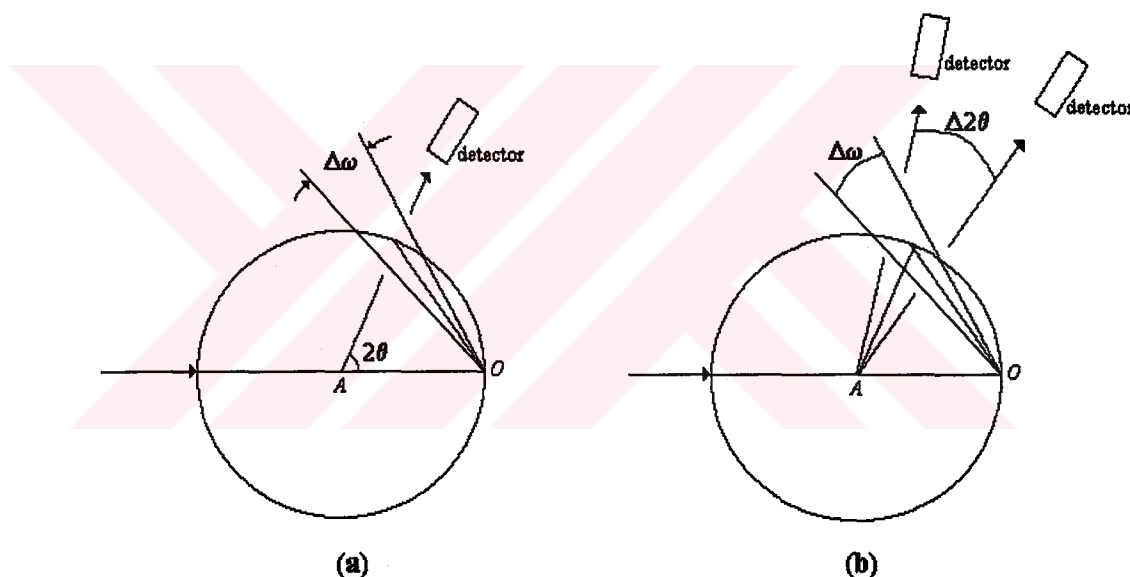


Figure 3.5 Diffractometer scan types. (a) w -scan (b) $w/2\theta$ -scan

3.4 Scattering of X-rays by a Crystal

An Argand diagram may represent the combination of waves. The waves are represented as vectors with real and imaginary components. We consider that the X-rays diffracted by structure with N atoms. The resultant of N waves is,

$$\vec{F} = f_1 e^{i\phi_1} + f_2 e^{i\phi_2} + \dots + f_j e^{i\phi_j} + \dots + f_N e^{i\phi_N} \quad (3.2)$$

$$\vec{F} = \sum_{j=1}^N f_j e^{i\phi_j} \quad (3.3)$$

On an Argand diagram, (3.3) expresses a polygon of vectors (Figure 3.6); the resultant \vec{F} is given by

$$\vec{F} = |F| e^{i\phi} \quad (3.4)$$

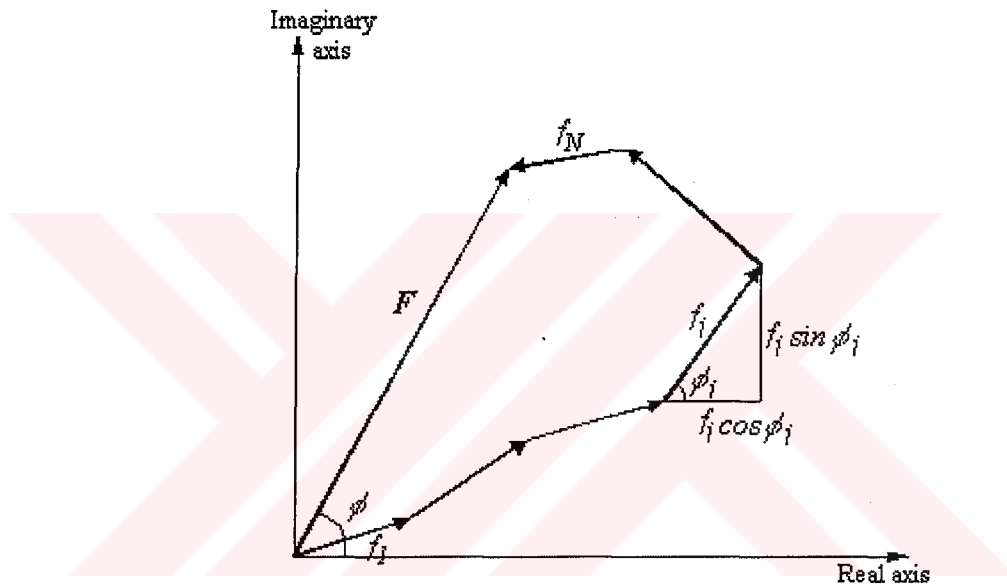


Figure 3.6 Combination of N waves on an Argand diagram.

The amplitude $|F|$ is given by

$$|F|^2 = \vec{F} \vec{F}^* \quad (3.5)$$

where \vec{F}^* is the complex conjugate of \vec{F} :

$$\vec{F}^* = |F| e^{-i\phi} \quad (3.6)$$

By analogy we can write,

$$|F| = (A^2 + B^2)^{1/2} \quad (3.7)$$

where

$$A = \sum_{j=1}^N f_j \cos \phi_j \quad \text{and} \quad B = \sum_{j=1}^N f_j \sin \phi_j \quad (3.8)$$

A and B are, respectively, the real and imaginary components of \vec{F} , and the phase angle ϕ is given by

$$\tan \phi = \frac{B}{A} \quad (3.9)$$

In unit cell if we consider a structure, which have fractional coordinates x_j, y_j, z_j ($j=1, 2, \dots, N$), the resultant of the path difference of the waves, which are scattered by j .th atom, is as follows

$$\delta_j = \lambda(hx_j + ky_j + lz_j) \quad (3.10)$$

The phase difference can be written as

$$\Phi_j = \left(\frac{2\pi}{\lambda}\right)\delta_j \quad \text{or} \quad \Phi_j = 2\pi(hx_j + ky_j + lz_j) \quad (3.11)$$

3.5 Crystal Structure Factor

In (3.2), F is called structure factor. The term structure factor is used to represent the scattering by the contents of one unit cell of a structure.

If we add (3.11) into (3.3); we can write

$$F_{hkl} = \sum_{j=1}^N f_j \exp[2\pi i(hx_j + ky_j + lz_j)] \quad (3.12)$$

for structure factor.

In order to evaluate the F_{hkl} , we need also f_j , called the atomic scattering factors. If we know their values, the calculation of atomic scattering factors is complicated. Because; "they are tabulated as functions of $\frac{\sin \theta}{\lambda}$, and denoted as f_j . The atomic scattering factor depends upon the nature of the atom. f_j depends upon the number of extra nuclear electrons in the atom: its maximum value for a given atom j is Z_j , the atomic number of the j .th atomic species." (Ladd&Palmer, 1988, pp.164).

The variation of f_j with $\frac{\sin \theta}{\lambda}$ is shown in Figure 3.7.

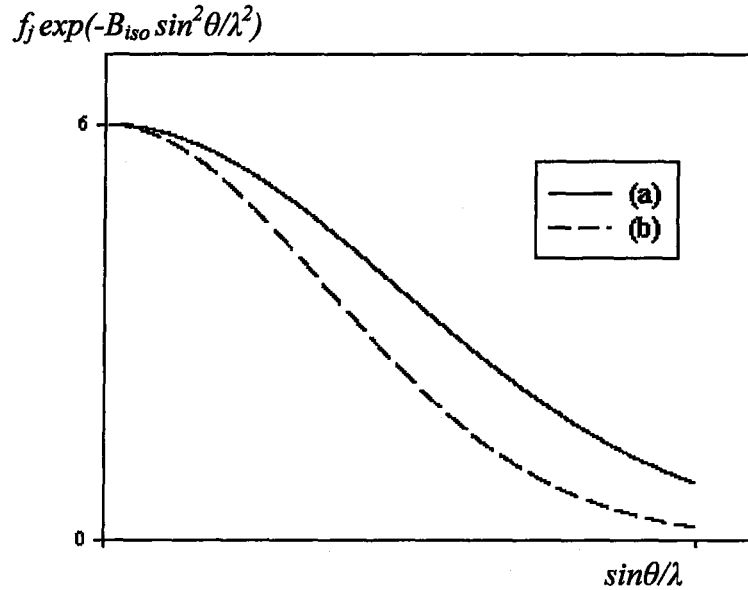


Figure 3.7 Atomic scattering factors: (a) stationary atom, (b) atom corrected for thermal vibration.

3.6 Fourier Synthesis and Electron Density

Electron's distribution around the atoms is presented electron density function. Because of three dimension periodicity's of the lattice, the electron density at the point (x, y, z) as $\rho(x, y, z)$ can be represented as a triple Fourier series. Than we may write

$$\rho(x, y, z) = \frac{1}{V} \sum_h \sum_k^{+\infty} \sum_l^{-\infty} F_{hkl} \exp[-2\pi i(hx + ky + lz)] \quad (3.13)$$

where V and F_{hkl} are the unit-cell volume and the structure factor, respectively. From (3.4) we can write

$$\Phi_{hkl} = \arctan \left[\frac{B_{hkl}}{A_{hkl}} \right] \quad (3.14)$$

where Φ_{hkl} is phase angle of crystal structure factor. From Friedel's law, which says, the diffraction patterns have a center of symmetry,

$$F_{hkl} = F_{\bar{h}\bar{k}\bar{l}} \text{ or } \Phi_{hkl} = \Phi_{\bar{h}\bar{k}\bar{l}} \quad (3.15)$$

if we unite (3.4) and (3.13) the electron density function can be written as

$$\rho(x, y, z) = \frac{1}{V} \sum_h \sum_k^{+\infty} \sum_l^{-\infty} F_{hkl} \exp[2\pi i(hx + ky + lz) + \Phi_{hkl}] \quad (3.16)$$

If we write this equation as trigonometric functions, the electron density function as follows

$$\rho(x, y, z) = \frac{1}{V} \sum_h \sum_k^{+\infty} \sum_l^{-\infty} |F_{hkl}| \cos[2\pi(hx + ky + lz) - \Phi_{hkl}] \quad (3.17)$$

As we can see from (3.16), if we know the structure factors, F_{hkl} , the electron densities can be calculated. The peaks at the electron density maps can be used for determining the atom's positions. The experimental measured diffraction intensities give the amplitude of crystal structure factors.

But we need the phases, Φ_{hkl} , for three dimensional electron density map. In this study, "direct methods" has been used in order to derive the phases.

3.7 The Phase Problem

There are several ways of describing the phase problem of crystallography:

"Both the phases and the magnitudes of the Bragg reflections must be known to form the image of the scattering material, but only the magnitudes are observed."

"It's a Catch-22 situation: atom positions can be calculated if phase information is known, and phase information can be calculated if atom positions are known."

“The phase problem makes the structure determination experiment become an indirect process of modeling the crystal; if the reflection intensities of the model match the measured values the model is assumed correct.”

“The phase problem is what makes crystallography fun: it puts an element of ‘puzzle solving’ into the structure determination experiment.”

In the structure determination experiment the phase problem makes the major hurdle that of getting the model structure started: the problem of how to use the large amount of experimental data obtained to begin deducing the atom arrangements which produce those data.

If the structure is centrosymmetric with the origin at the center of symmetry, the phase angle, Φ_{hkl} , for each reflection must be 0° or 180° . Thus

$$F_{hkl} = |F_{hkl}| \cos(\Phi_{hkl}) = \pm |F_{hkl}| \quad (3.18)$$

and the phase problem becomes the problem of determining the correct sign for each of the thousands of structure factor amplitudes that were measured. For n unique reflections, the number of combinations of phases possible is 2^n .

If the structure is not centrosymmetric the phase angle can have any value ranging over an entire circle. Assuming the phase angles need to be known within $\pm 45^\circ$ in order to get a sufficiently good image of the structure. The number of possible phase angle combinations becomes 4^n .

Reflection intensities are the focus of the front end of the structure determination experiment (data collection) and the F or F^2 values are the focus of the later part of the experiment (least-squares refinement). With this emphasis on reflection amplitude it is important to note that the phase information can be more important than the amplitude data for the determination of the structure (Lecture Notes, 2001, pp.XV-1).

3.8 Data Reduction

The general process of converting electronic measurements into usable diffraction data is called "data reduction". For each intensity maxima, data reduction includes an integration of the peak including corrections for the spot shape, subtraction of the relative background intensity, corrections for the geometry of the instrument, corrections for crystal decay, and averaging or merging of equivalent data.

The first step involves both an integration of the peak and a subtraction of the background. The integration step must include corrections for overly strong peaks that have been recollected at shorter times or with attenuators. This step sometimes includes corrections for the shape of the diffraction spot. The background, that is presumed to run beneath the peak measurement, is measured both before and after the peak or is sampled in various areas around the peak. Background scattering may be due to scattering from the sample mount, scattering from air, fluorescence radiation from the sample or mount, and cosmic radiation. This step produces both raw intensities and estimates of the standard uncertainties, often called estimated standard deviations, in the intensities. The standard uncertainties that calculated directly from counting statistics were found to be underestimates of the true uncertainties. Now standard uncertainties in intensities include a small "instrument instability" correction term. The following expression is usually applied in calculating structure factor amplitudes.

$$I_{hkl} = K.L.p.T.A.E.|F_{hkl}|^2 \quad (3.19)$$

In this equation, the symbols indicate;

K: scale factor

L: Lorentz factor

p: Polarization factor

T: Debye-Waller Temperature factor

A: Absorption factor

E: Extinction factor

To use in crystal structure analysis, diffraction intensities that are measured must be corrected by these factors so that F_{hkl} values are gained.

3.8.1 Lorentz Correction

Some peaks, such as those peaks near to the rotation axis, spend more time passing through the Ewald sphere of reflection than do others. This difference in time is corrected by a term called the Lorentz factor. For point detector systems performing ω - 2θ or ω scans, this correction is simply

$$L = \frac{1}{(\sin 2\theta)} \quad (3.20)$$

Area detector intensities are generally not located in the horizontal plane, so different formulas are used that is based upon whether the data are being collected using ω or f scans.

3.8.2 Polarization Correction

At different scattering angles the scattered beam will be attenuated by the polarization of the beam by the sample. If the incident radiation is plane polarized (random orientation of the electric vector of the radiation) then the polarization correction is given by

$$p = \frac{1}{2}(1 + \cos^2 2\theta) \quad (3.21)$$

If a monochromator is inserted in the incident beam, then the X-rays impinging on the sample are already partially polarized from the monochromator crystal and a different formula is used that depends upon the geometry of the monochromator.

3.8.3 Absorption Correction

The absorption of X-rays follows Beer's Law:

$$I = I_0 \exp(-\mu x) \quad (3.22)$$

where I is transmitted intensity, I_0 is incident intensity, x is thickness of material, μ is linear absorption coefficient of the material. The linear absorption coefficient depends on the substance, its density, and the wavelength of radiation. Since μ

depends on the density of the absorbing material, it is usually tabulated as the mass absorption coefficient $\mu_m = \left(\frac{\mu}{\rho}\right)$. The linear absorption coefficient is then calculated from the formula:

$$\mu = \rho \left(\frac{P_n}{100} \right) \left(\frac{\mu}{\rho} \right)_n \quad (3.23)$$

where the summation is carried out over the n atom types in the cell, P_n is the percent by mass of the given atom type in the cell and ρ is the density of the crystal. The absorption coefficients for crystals in this study are found 0.1018 mm^{-1} for $C_{28}H_{24}N_2O_4$ and 1.7905 mm^{-1} for $C_{23}H_{32}N_4Se$ from Table 3.1 and Table 3.2, respectively.

Table 3.1 Atomic mass and mass absorption coefficients for $C_{28}H_{24}N_2O_4$.

Atom	Number of atoms	Atomic mass m (a.m.u.)	Total mass (a.m.u.)	Percent (%) P_n	Mass absorption coefficient (MoK $_{\alpha}$) (cm^2/g)
C	28	12.01	336.28	74.30	0.70
H	24	1.01	24.24	5.35	0.37
N	2	14.01	28.02	6.19	1.10
O	4	16.00	64.00	14.14	1.50

Table 3.2 Atomic mass and mass absorption coefficients for $C_{23}H_{32}N_4Se$.

Atom	Number of atoms	Atomic mass m (a.m.u.)	Total mass (a.m.u.)	Percent (%) P_n	Mass absorption coefficient (MoK $_{\alpha}$) (cm^2/g)
C	23	12.01	276.23	62.27	0.70
H	32	1.01	32.32	7.28	0.37
N	4	14.01	56.04	12.63	1.10
Se	1	78.96	78.96	17.80	74.0

$$\text{For } C_{28}H_{24}N_2O_4 \quad \sum_n m_n = 452.54, \rho = 1.32 \text{ g/cm}^3, \sum_n \left(\frac{P_n}{100} \right) \left(\frac{\mu}{\rho} \right)_n = 0.77179$$

$$\text{For } C_{23}H_{32}N_4Se \quad \sum_n m_n = 443.55, \rho = 1.30 \text{ g/cm}^3, \sum_n \left(\frac{P_n}{100} \right) \left(\frac{\mu}{\rho} \right)_n = 13.773$$

According to these results, the linear absorption coefficients of crystals are found $\mu = 0.1018 \text{ mm}^{-1}$ for $C_{28}H_{24}N_2O_4$ and $\mu = 1.7905 \text{ mm}^{-1}$ for $C_{23}H_{32}N_4Se$ from (3.23).

Absorption of X-rays by the sample is often the most difficult correction to perform. The extent of absorption depends on the size and shape of the crystal as well as the types and relative amounts of different atoms in the sample, and the wavelength of radiation used in the experiment. Also absorption from the sample mount may need to be included in the correction. Most researchers try to reduce the effects of absorption by reshaping the sample, properly mounting the sample, using a smaller crystal, or by using a higher energy radiation. There are four general classes of absorption corrections, analytical, empirical, geometrical, and Fourier.

3.8.4 Debye-Waller Temperature Factor Correction

Thermal motion affects X-rays intensities. Normal scattering factor curves is calculated through the electron distribution that belongs to a fix atom. But, in fact, atoms in the crystal vibrate continuously around their points. The magnitude of vibration depends on temperature, atom's mass and interaction forces, which are taken place by perimeter atoms. Vibration is usually so high at high temperatures. Thermal motion causes that electron cloud is located into larger volume and this case causes that scattering power of real atom decreases rapidly (Figure 3.7). The variation of scattering power can be written as

$$\exp\left(-B \frac{\sin^2 \theta}{\lambda^2}\right) \quad (3.24)$$

where B is isotropic temperature factor and is proportional to the average of atomic vibration amplitude's square $(\overline{u^2})$ (Aygün, 1997).

$$B = 8\pi^2 \overline{u^2} \quad (3.25)$$

so, scattering factor for a real atom as follows

$$f = f_o \exp\left(-B \frac{\sin^2 \theta}{\lambda^2}\right) \quad (3.26)$$

where f_o is scattering amplitude at 0 K and f is scattering factor at laboratory temperature. After the Lorentz-polarization ($L-p$) correction is done, observed average intensity becomes

$$\overline{I}_{obs} = \left\langle |F_{obs}|^2 \right\rangle_{ave} \quad (3.27)$$

Theoretical average intensity for a structure with N atoms in the unit-cell is

$$\overline{I}_{cal} = \sum_{i=1}^N f_i^2 \quad (3.28)$$

If we unite (3.26) and (3.28),

$$\overline{I}_{obs} = \sum_{i=1}^N f_{oi}^2 \exp\left(-B \frac{\sin^2 \theta}{\lambda^2}\right) \quad (3.29)$$

here B is constant for all atoms and can be calculated. Than, we can write

$$\overline{I}_{obs} = \exp\left(-B \frac{\sin^2 \theta}{\lambda^2}\right) \sum_{i=1}^N f_{oi}^2 \quad (3.30)$$

In addition,

$$\overline{I}_{cal} = C \overline{I}_{obs} \quad (3.31)$$

$$\overline{I}_{cal} = C \exp\left(-B \frac{\sin^2 \theta}{\lambda^2}\right) \sum_{i=1}^N f_{oi}^2 \quad (3.32)$$

$$\ln \left[\frac{\overline{I}_{cal}}{\sum_{i=1}^N f_{oi}^2} \right] = \ln C - \left[2B \frac{\sin^2 \theta}{\lambda^2} \right] \quad (3.33)$$

The variation of $\ln \left[\frac{\overline{I}_{cal}}{\sum_{i=1}^N f_{oi}^2} \right]$ with $\frac{\sin^2 \theta}{\lambda^2}$ is shown in Figure 3.8. So we can find

the isotropic temperature factor, B , from the slop of the graphic.

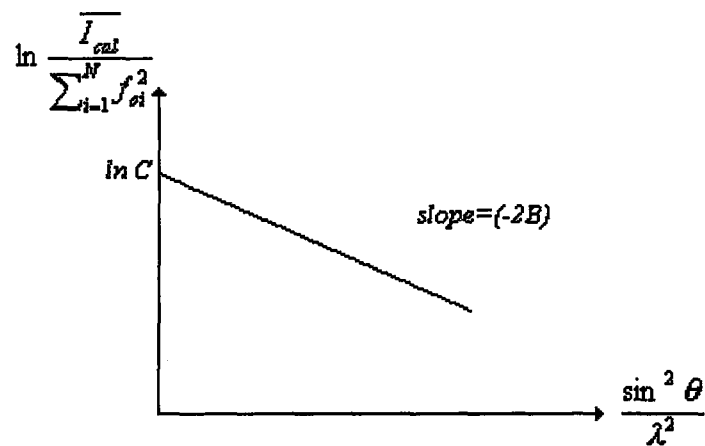


Figure 3.8 Wilson plot.

Here C depends on k that is scale constant between $|F_{obs}|$ and $|F_{cal}|$, and can be written as

$$k = \frac{1}{\sqrt{C}} \quad \text{or} \quad |F_{obs}| = k|F_{cal}| \quad (3.34)$$

3.8.5 Extinction Correction

The extinction correction, E , is not automatically applied although the program will often prompt when one might be necessary. Real crystals can be envisaged as a mosaic of crystalline blocks, each block tilted very slightly with respect to the others and separated by cracks and faults. When an X-ray beam is diffracted by underlying blocks; thus the underlying blocks contribute less than expected to the overall effect. The above manifestation of extinction can be detected when $|F_{obs}|$ is less than $|F_{cal}|$, particularly for very intense reflections. The correction then involves rescaling to make the most intense Bragg reflections agree with those calculated.

3.8.6 Anomalous Scattering Factor

In discussing the scattering of X-rays by atoms, we have implicitly assumed that the frequency of the radiation used was far from that corresponding to any electronic transition in the atoms being irradiated. But when this condition does not hold, the

scattering factor for that atom is no longer a scalar, but rather becomes a complex. This situation is called “anomalous scattering” or “anomalous dispersion”. If we write an expression for scattering factor:

$$f = f_o + \Delta f' + i\Delta f'' \quad (3.35)$$

where $\Delta f'$ is a real correction, usually negative, and $\Delta f''$ is imaginary component respect to f_o and $\Delta f'$. A possible situation is illustrated for normal case in Figure 3.9 (a) and for anomalous case in Figure 3.9 (b).

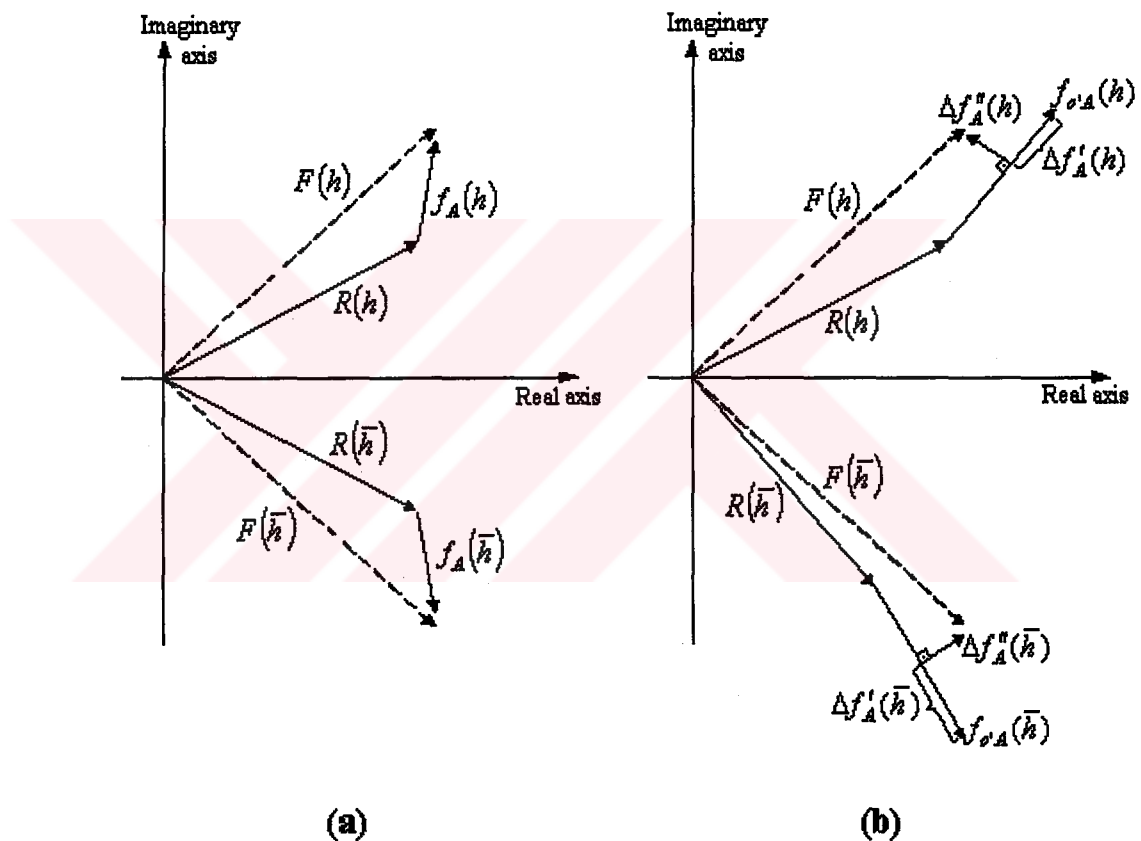


Figure 3.9 Anomalous scattering of atom A with respect to the rest of the structure

R: (a) normal case- $|F(h)| = |F(\bar{h})|$; (b) anomalous case- $|F(h)| \neq |F(\bar{h})|$.

CHAPTER FOUR

SOLUTION OF CRYSTAL STRUCTURE

4.1 Introduction

The success-controlling step of a structure determination is normally the step of finding the correct locations for the first atoms of the model structure: once model is launched, the techniques for adding atoms to the trial structure (Fourier techniques) and refining the structure (least-squares or Fourier methods) are more straightforward procedures. The necessary start for a model can be just a single atom in the case of a heavy-atom in the small molecule in the case of organic-type structures.

The number of techniques used for the initiation of a small molecule model is not large.

4.1.1 The trial-and-error method:

This method was about the only approach available in the 1920's and 1930's. One part of the research was to find crystals, which had most, or all, of the atoms located in special positions of highly symmetric space groups. In this way the choices for the atom positions were limited. The description by Linus Pauling of the structural research done in 1920's at Cal Tech provides interesting insights into this era of crystallography.

4.1.2 The Patterson Technique:

This technique was the dominant method used in structure determination research from the mid-1930's until the mid-1960's. This approach, which is still in use, requires no phase information and uses all of the reflection data. The method involves the unraveling of a map of inter-atomic vectors to determine the atom arrangement, which produced the vector pattern. A Patterson map contains too many vectors to unscramble if the number of unique atoms is greater than about 20, unless one or more of the atoms are significantly heavier than the others. In this case the vectors involving the heavy atoms dominate the vector map and can be used to locate the heavy atoms in the unit-cell.

The last method which took place in 1960's and 1970's, and has been used in this study, "direct methods", will be discussed at length in a following sections.

4.2 Direct Methods

4.2.1 Background and Early History

With the term "direct methods" are the methods which try to derive the phases of a set of structure factors directly from the magnitudes through mathematical relationships. These magnitudes are calculated readily from the observed intensities, knowledge of the size and symmetry of the unit-cell, and the chemical composition of the substance being studied. In the case of X-ray diffraction, it is possible to relate the phase and the magnitude of a way, two important properties of the electron density function should be considered:

1. it is everywhere positive, $\rho(r) > 0$ (positivity);
2. it is composed of isolated spherical atoms (atomicity).

This means that the number of parameters to be determined is an order of magnitude smaller than the number of observations.

Historically the first mathematical relationships capable of giving phase information were obtained, in the form of inequalities, by Harker and Kasper and by Gillis in the late 1940s and early 1950s. Some of these inequalities provided unambiguous phase relationships for the centrosymmetric decaborane structure, with Harker and Kasper solved with their aid, but the Harker-Kasper approach had no great impact initially, because it was limited in practice to rather simple centrosymmetric structures. Gillis made the important point that, even when the inequalities could not define the sign of a particular structure factor, they might imply a sign if the inequality was nearly satisfied. The next important advance was by Karle and Hauptman in 1950, dealing again with inequalities but in a more general and eventually fruitful way. They showed that inequalities restrict the range of phase angles for a non-centrosymmetric structure. In 1952 Sayre considered that for a structure formed by well resolved and almost equal atoms, the two functions $g(r)$ and $g^2(r)$ are quite similar and show maxima at the same positions. Cochran, and independently Zachariasen, arrived at relations among the signs of structure factors of three related reflections, relations that were shown to have a high probability of being valid. The relation among the indices of any three reflections was that the indices of one of them must be expressible as the sum of the indices of the other two. The relation was called a triple-product sign relationship, or *TPSR*, because if we let H represent a reflection (h,k,l) , K represent (h',k',l') , and s be “the sign of the structure factor of”, then the product of the signs of H , K and $(H+K)$ is very likely to be positive:

$$s(H).s(K).s(H + K) \approx + \quad (4.1)$$

It turns out that, for most structures, one needs good approximations to the phases of only about 10 percent of the observed reflections to get a recognizable picture of the structure from an “E-map”, which is a three-dimensional Fourier synthesis calculated with E_{hkl} rather than F_{hkl} . Because the method is successful even when there are some errors in the initial phases, it is not necessary in applying direct methods that all the assumptions made in deriving the equations used be fulfilled exactly. The errors in phases are reduced as the image of the molecule is improved

through successive E-maps and F-maps, and as refinement proceeds by least-squares or other methods are used.

Many people contributed to the development of direct methods, but the key significant of the contributions of Herbert Hauptman (mathematician) and Jerome Karle (physicist) was recognized by the award to them of the Nobel Prize for Chemistry in 1985.

4.2.2 Normalized Structure Factors and Intensity Statistics

Some structure factors that correspond to a net scattering from a few atoms more or less in phase, so that $|F_{hkl}|$ is a non-negligible fraction of what it would be if many atoms scattered in phase. There is always a certain proportion of such reflections in any structure, but it is not usually obvious which reflections these are, because of the rapid decline in atomic scattering power (for X-rays) with increasing scattering angle and with temperature. However, correction for these effects is straightforward, and is the essential step in the calculation of normalized structure factor magnitudes ($|E_{hkl}|$), which represent the ratio of the $|F_{hkl}|$ to its expectation value at the $\sin\theta/\lambda$ for that hkl . Each $|F_{hkl}|$ is converted to the corresponding $|E_{hkl}|$ by dividing by rms value of the atomic scattering factors in the structure, at the value of $\sin\theta/\lambda$ corresponding to that hkl , and by the average temperature factor for the atoms in the structure:

$$E_{hkl} = \frac{|F_{hkl}|}{\Sigma} \quad (4.2)$$

where $\Sigma = \sqrt{\varepsilon \sum_j f_j^2 \exp\left[-B \frac{\sin^2 \theta}{\lambda^2}\right]}$, with B an average isotropic temperature factor.

Central Limit Theorem states that the distribution of a sum of n independent random variables tends, as n goes to infinity, to a normal or Gaussian distribution function. The normal or Gaussian distribution function is given by

$$p(x) = \frac{1}{\sigma\sqrt{2\pi}} \exp\left[-\frac{(x-m)^2}{2\sigma^2}\right] \quad (4.3)$$

where m is the mean and σ is the standard deviation.

If the atoms in a crystal are considered to be arranged randomly, and the number of atoms is large, the Central Limit Theorem can be applied to the distribution of the intensities of diffraction from the crystal, since that intensity depends on F_{hkl}^2 , and F_{hkl} is just the sum of the scattering from many randomly distributed atoms. When the calculation is made for $|E_{hkl}|$ values instead of $|F_{hkl}|$'s, the results are particularly simple, since the distribution of $|E_{hkl}|$ is Gaussian. Table 4.1 presents some useful results for the equal-atom case.

Table 4.1 Some statistical properties of normalized structure factor magnitudes*.

	Non-centrosymmetric	Centrosymmetric	Hypercentric [#]
$\langle E \rangle$	0.886	0.798	0.718
$\langle E ^2 \rangle$	1.000	1.000	1.000
$\langle E^2 - 1 \rangle$	0.736	0.968	1.145

* The symbol $\langle \rangle$ represents an average overall hkl .

[#] The hypercentric distribution applies to structures containing centrosymmetric molecules that lie in general positions in centrosymmetric space groups.

4.2.3 Centrosymmetric Structures

The phase problem of centrosymmetric structures can be solved easier than non-centrosymmetric structures. There are only two possible phase angles for the former, rather than a complete range over a circle. We thus focus first on structures with a center of symmetry.

The first stage in any direct methods approach is calculating the $|E_{hkl}|$'s. After the $|E_{hkl}|$'s have been sorted on their magnitudes, the kinds of statistical information contained in Table 4.1 are calculated, to provide an indication of whether or not the structure is centrosymmetric. The next step is to assign up to three signs of reflections arbitrarily, in order to fix one of the equivalent centers of symmetry as the origin of the unit-cell. This is needed because, although changing the origin leaves the magnitudes of the F_{hkl} 's unaltered, it may change phases. The indices of the reflections must not be all even (*eee*), since no change of origin will affect the sign of an *eee* reflection, and they must be linearly independent with respect to this property.

At this point, one (manually, computer program) starts to search for TPSRs (triple-product sign relationship). The probability that a triple-product is positive is given approximately by

$$P_+ = \frac{1}{2} + \frac{1}{2} \tanh \left[\frac{|E_H E_K E_{H-K}|}{\sqrt{N}} \right] \quad (4.4)$$

and the probability that E_H itself is positive is given by

$$P_+ = \frac{1}{2} + \frac{1}{2} \tanh \left[N^{-1/2} \left(|E_H| \sum_K E_K E_{H-K} \right) \right] \quad (4.5)$$

with N the number of atoms in the unit-cell. After the program searches for all sets triple-products among the E values to be used, it evaluates the probability that each of these triple-products is positive, and that the individual values of E are positive, and uses these probabilities in deciding how to proceed further.

4.2.4 Non-centrosymmetric Structures

As with centrosymmetric structures, one starts by assigning up to three phases of reflections arbitrarily. A fourth can usually be assigned also, to fix the enantiomorph, although not in all space groups. Initial estimates of additional phases are usually made with the 'tangent formula' of Karle and Hauptman:

$$\tan(\Phi_H) \approx \frac{\sum_K \kappa_{H,K} \sin[\Phi_K + \Phi_{H-K}]}{\sum_K \kappa_{H,K} \cos[\Phi_K + \Phi_{H-K}]} \quad (4.6)$$

with κ a known function of the atomic numbers of the atoms present and of the magnitudes of the E values for reflections H , K , and $(-H-K)$. The tangent formula is used for extending phases, and there are other relations, including equations for estimating the probability that a phase angle is correct, quite analogous to those used for finding signs for centrosymmetric structures (Lecture Notes, 2001).

$$\Phi_H = \Phi_K + \Phi_{H-K} \quad (4.7)$$

One of the currently most used direct methods programs is *SHELXS-97*, which is used in this study. It finds a number of possible solutions but it tries hard to identify the correct solution, which it then attempts to improve by using E-maps and a partial-structure recycling procedure.

4.2.5 Criteria of Correctness Set of Phases

Phase determination has usually given more than one solution. For a few sets of given phases, calculating and interpreting of electron density maps that help to perceive right structure corresponding to these sets of phase have a long time. Instead of, computing some of appropriate functions which are referred to as criteria of correctness set of phases or “figures of merit” (FOM) is easier than other ways. FOM, makes possible the fact that correctness of each sets of phase is precedingly estimated. Some of the FOMs are MABS, NQUAL, R_α , CPHASE, ψ_0 , ... Let us investigate prevalently used of them.

4.2.5.1 MABS

It is defined as

$$MABS = \frac{\sum_h \alpha_h}{\sum_h \langle \alpha_h \rangle} = \frac{A}{A_e} \quad (4.8)$$

which triplet relations studied in estimation of phase are connected with dependence among relations in question. In order to obtain correct structure, A_e that is theoretically estimated and A close on each other and MABS is approximately equal to 1. In practice, for approaching to right phase set A must be bigger than A_e and values of MABS must be ranging from 0.9 to 1.3.

4.2.5.2 NQUAL

It is defined as

$$NQUAL = \frac{\sum [\sum (E_1 E_2) \sum (E_3 E_4 E_5)]}{\sum [|\sum (E_1 E_2)| |\sum (E_3 E_4 E_5)|]} \quad (4.9)$$

For right structure solution, the value of NQUAL must be close to -1. for random phases, it is equal to zero.

4.2.5.3 R_α FOM

It is defined as

$$R_\alpha = \frac{100}{A_e} \left(\sum_h |\alpha_h - \langle \alpha_h \rangle| \right) \quad (4.10)$$

which this kind of fom proportionates with number of triplet that deviate from its expected statistical distribution. For right set of phases, this value have to be minimum. By computing different foms for each sets of phase deriving combined criterion correctness sets of phase (combined figure of merit, CFOM) is very useful. CFOM is more effective than other functions in separating sets of suitable phase. Minimum values of CFOM put forward that set of phase is true.

CHAPTER FIVE
CRYSTAL STRUCTURE
REFINEMENT

5.1 Refinement Methods

When an approximate structure has been obtained using direct, Patterson or other methods, the atomic parameters that were determined with this method can be refined. Additional atoms can be located and their parameters also refined. These additional atoms are found using the Fourier synthesis method.

Two methods have been used for the refinement of the atomic positions and displacement (or temperature) parameters. One method is based on Fourier techniques, so called “Difference Fourier Method”, and the other is based on least-squares techniques, so called “Least-Squares Method”.

5.1.1 Difference Fourier Method

One way of the completing and refining a structural model is the “difference Fourier synthesis method”. In this method, we investigate the difference between experimental and calculated electron densities. We can write,

$$\rho_{cal}(\vec{r}) = \frac{1}{V} \sum_h \sum_k \sum_l F_{hkl}^{cal} \exp(-2\pi i \vec{h} \cdot \vec{r}) \quad (5.1)$$

for calculated electron density,

$$\rho_{obs}(\vec{r}) = \frac{1}{V} \sum_h \sum_k \sum_l F_{hkl}^{obs} \exp(-2\pi i \vec{h} \cdot \vec{r}) \quad (5.2)$$

for experimental electron density. In order to see how much the initial model deviates from the real structure, the difference series

$$\begin{aligned}\Delta\rho(\vec{r}) &= \rho_{obs}(\vec{r}) - \rho_{cal}(\vec{r}) \\ &= \frac{1}{V} \sum_h \sum_k \sum_l [F_{hkl}^{obs} - F_{hkl}^{cal}] \exp(-2\pi i \vec{h} \cdot \vec{r})\end{aligned}\quad (5.3)$$

should be computed where F_{hkl}^{obs} and F_{hkl}^{cal} can be written as follows

$$F_{hkl}^{obs} = |F_{hkl}^{obs}| \exp(i\Phi^{obs}) \quad \text{and} \quad F_{hkl}^{cal} = |F_{hkl}^{cal}| \exp(i\Phi^{cal}) \quad (5.4)$$

Unfortunately the values of Φ^{obs} are not known and we have to assume $\Phi^{obs} \approx \Phi^{cal}$, will hold better the better is the initial model. (5.3) then becomes

$$\Delta\rho(\vec{r}) = \frac{1}{V} \sum_h \sum_k \sum_l [|F_{hkl}^{obs}| - |F_{hkl}^{cal}|] \exp(-2\pi i \vec{h} \cdot \vec{r} + i\Phi^{cal}) \quad (5.5)$$

If in the model an atom is missing, then $\rho_{cal}(\vec{r})$ will be zero at the corresponding position, while $\rho_{obs}(\vec{r})$ will show a maximum. The difference synthesis will also show a peak at the same position but it will be almost zero at the positions of model atoms where $\rho_{obs}(\vec{r}) \approx \rho_{cal}(\vec{r})$.

5.1.2 Least-Squares Method

By far the most widely used method of structure refinement is the “least-squares method”. The crystallographic problem of determining the best set of atomic parameters that can be obtained from a set of experimental structure factors is usually solved with this method.

We can write the calculated structure factor, for a better set of atomic coordinates and temperature factors,

$$F_{hkl}^{cal} = \sum_{j=1}^{N/2} 2f_j \left(-B_j \frac{\sin^2 \theta}{\lambda^2} \right) \cos[2\pi(hx_j + ky_j + lz_j)] \quad (5.6)$$

where the structure is centrosymmetric and the temperature factor is isotropic. The correct values of parameters for j.th atom is as follows:

$$(B_j + \Delta B_j, x_j + \Delta x_j, y_j + \Delta y_j, z_j + \Delta z_j) \quad (5.7)$$

and the observed structure factor can be written as

$$F_{hkl}^{obs} = \sum_{j=1}^{N/2} 2f_j \exp \left[- (B_j + \Delta B_j) \frac{\sin^2 \theta}{\lambda^2} \right] \cos [2\pi \{h(x_j + \Delta x_j) + k(y_j + \Delta y_j) + l(z_j + \Delta z_j)\}] \quad (5.8)$$

The difference of two expressions

$$\begin{aligned} \Delta F_{hkl} &= F_{hkl}^{obs} - F_{hkl}^{cal} \\ &= \sum_{j=1}^{N/2} \left(\frac{\partial F_{hkl}^{cal}}{\partial B_j} \Delta B_j + \frac{\partial F_{hkl}^{cal}}{\partial x_j} \Delta x_j + \frac{\partial F_{hkl}^{cal}}{\partial y_j} \Delta y_j + \frac{\partial F_{hkl}^{cal}}{\partial z_j} \Delta z_j \right) \end{aligned} \quad (5.9)$$

In order of to gain the best approximation for observed structure factors, which are assumed to have no error in practice, the following expression must be minimum.

$$R_s = \sum_h [F_{hkl}^{obs} - F_{hkl}^{cal}]^2 \approx 0 \quad (5.10)$$

5.1.2.1 Overall Strategy:

The overall strategy for crystallographic least-squares refinement depends on the size and nature of the problem, but some techniques can be mentioned here.

1. At the start of the refinement, the number of parameters should be minimized by refining only position and isotropic displacement parameters for the atoms that have been found from direct or Patterson methods (Section 5.1 and 5.2).
2. From a difference electron density map (Section 4.6), other non-hydrogen atoms can be found and included in the refinement.
3. Anisotropic displacement parameters for the non-hydrogen atoms can be added. Hydrogen atoms cannot always be observed in difference electron density maps. However, hydrogen atoms can be placed at appropriate positions by using "riding" model constrains.
4. A final difference electron density map should always be calculated, to insure that no significant features of the structure have been left out of the refinement. Special attention should be given to possible disorder (large atomic displacement parameters for some atoms might be a clue), solvent

molecules left out of the refinement or atoms (including hydrogen) that have been misplaced.

5. The estimated standard deviation and correlation coefficients for the refined parameters are calculated for the final refinement cycle.

5.2 Error Analysis

5.2.1 R Factors

Crystallographers often look first for the R-value as one of the simplest ways of evaluating the general results of a structural refinement. “R-value” shows the sensitivity between experimental and calculated data and can be written as

$$R = \frac{\sum_h \sum_k \sum_l |\Delta F_{hkl}|}{\sum_h \sum_k \sum_l |F_{hkl}^{obs}|} \quad \text{where} \quad \Delta F_{hkl} = |F_{hkl}^{obs}| - |F_{hkl}^{cal}|. \quad (5.11)$$

R-values ranges 0.4 – 0.5 at the starting of refinement and 0.02 – 0.06 at the end of the refinement.

Another R factor is R_w -value; called weighted R-value is given by

$$R_w = \sqrt{\frac{\sum_h \sum_k \sum_l w(\Delta F)^2}{\sum_h \sum_k \sum_l w|F_{hkl}^{obs}|^2}} \quad (5.12)$$

where w is the weight function.

5.2.2 Goodness of Fit

Another index obtained from the least-squares refinement is the “Goodness of Fit”,

$$GOF = \sqrt{\frac{\sum_h \sum_k \sum_l w[(F_{hkl}^{cal})^2 - (F_{hkl}^{obs})^2]^2}{(n - m)}} \quad (5.13)$$

which is a measure of how well the distribution ΔF values fit the distribution expected for the weight which were used. Here n is the number reflections and m is the number of variables refined. GOF value must be nearly 1.0 in a perfect situation.

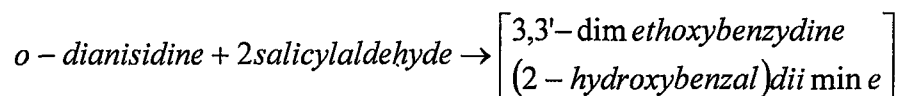
5.2.3 Final Difference Map

The final difference map provides a real-space counterpart for checking how well the refined the model fits the experimental data, thus complimenting the R-factor which is a reciprocal-space measure. The final difference map should be featureless, with no peaks or holes of a magnitude greater than a few estimated standard deviations of the map values.

5.2.4 Estimated Standard Deviations

Also we search for sensitivity of atomic parameters at the end of determination. In order to determine the structure sensitively, the standard deviations must be less than 0.001 for coordinates, 0.01Å for bond distances and 1° for angles.

A typical procedure for preparation is given.



3,3'-dimethoxybenzidine(2-hydroxybenzaldehyde)diimine was prepared by adding salicylaldehyde to the o-dianisidine (2:1 molar ratio) in hot dry ethanol which, after concentration and cooling, gave the required Schiff base ligand (Holm et al., 1966). $C_{28}H_{24}N_2O_4$, 452.5086 g/mol, 0.9046 g (99.95%), orange, needle, 163°C, $[M^+]$ 452.

6.1.2 Data Collection of $C_{28}H_{24}N_2O_4$ Crystal

Before starting data collection, the suitable crystals were selected from the synthesized crystals by using stereomicroscope and polarization microscope. Then a sample of size 0.08x0.24x0.36 mm³ was selected for the crystallographic study.

The diffraction measurements were performed at room temperature (293K) on an Enraf-Nonius CAD-4 diffractometer using graphite-monochromated MoK_α radiation. Orientation matrix and unit cell parameters were obtained from the setting angles of 25 reflections at medium θ ($0.66^\circ < \theta < 21.63^\circ$). The systematic absences and intensity symmetries indicated the monoclinic $C2/c$ space group. A total of 2325 intensities with $\theta_{max}=26.33^\circ$ were collected in the $\omega/2\theta$ scan mode, as suggested by peak-shape analysis. The crystal and equipment stabilities were checked by the intensities of three standard reflections monitored every 120 minutes. No significant intensity decay was observed (1.9%). The intensities were corrected for Lorentz and Polarization factors, but not for absorption effect ($\mu = 0.089 \text{ mm}^{-1}$).

6.1.3 Structure Solution & Refinement of $C_{28}H_{24}N_2O_4$ Crystal

The structure was solved by direct methods using *SHELXS-97* for 1685 reflections with $I > 2\sigma(I)$ and FOM values that used in phase determination are given in Table 6.1. Since the $\langle |E^2 - 1| \rangle = 1.056$, structure is centrosymmetric. The refinement (on F) was carried out by full-matrix least-squares method on the positional and anisotropic temperature parameters of the non-hydrogen atoms. The structure was refined to $R = 0.056$ for the observed reflections and $R = 0.078$ for all data. The maximum and minimum peaks, observed in the final $\Delta\rho$ map, were 0.180 and $-0.202 e\text{\AA}^{-3}$, respectively. The scattering factors were taken from *SHELXL-97*. All of the H atoms were found in the difference-Fourier maps, and positions and isotropic thermal parameters were refined. The C-H bond distances range from 0.93(3) to 1.02(3), while U_{iso} values for H atoms are in the range 0.048(5)-0.120(1).

Table 6.1 FOM values for $C_{28}H_{24}N_2O_4$.

Set Code	R_α	NQUAL	MABS	CFOM
1353721	0.035	-0.858	0.998	0.043

6.1.4 Experimental Results for $C_{28}H_{24}N_2O_4$ Crystal

Table 6.2 Crystallographic data for $C_{28}H_{24}N_2O_4$.

Crystal Data	
Chemical formula	$C_{28}H_{24}N_2O_4$
Color/shape	orange/needle
Formula weight (<i>a.m.u.</i>)	452.49
Space group	$C2/c$ (No.15)
Crystal system	Monoclinic
a, b, c (Å)	18.045(2), 11.725(4), 12.436(6)

$\alpha, \beta, \gamma (^{\circ})$	90, 120.03(3), 90
Cell volume (\AA^3)	2278.0(14)
Formula unit cell (Z)	4
D_x (g/cm^3)	1.32
F_{000}	952
Absorption coefficient μ (mm^{-1})	0.089
Crystal size (mm^3)	0.08x0.24x0.36

Data Collection	
Diffractometer	Enraf-Nonius CAD-4
Temperature (K)	293(2)
Scan type	$w/2\theta$
Radiation/Wavelength (\AA)	MoK $_{\alpha}$ /0.71070
Reflections measured	2325
Independent/ Observed reflections	2325/1685
Range of h, k, l	0 \rightarrow 22, 0 \rightarrow 14, -15 \rightarrow 13
Standard reflections	3
Standards interval time (min)	120
Standards decay %	1.9

Refinement	
Data/Restraints/Parameters	2325/0/203
Extinction Coefficient	0.0075(17)
Final R indices $[I > 2\sigma(I)]$	$R_1 = 0.056, wR_2 = 0.167$
R indices (all data)	$R_1 = 0.078, wR_2 = 0.182$

$GOF (onF^2)$	1.088
$\Delta\rho_{\min} / \Delta\rho_{\max} (e/\text{\AA}^3)$	-0.202/0.180
$(\Delta/\sigma)_{\max}$	0.003
Weighting function	$w = [\sigma^2(F_{obs}^2) + (0.1084P)^2 + 0.3065P]^{-1}$ $P = \frac{1}{3}(F_{obs}^2 + 2F_{cal}^2)$

Table 6.3 Atomic coordinates and equivalent isotropic thermal parameters (\AA^2).

Atom	<i>x</i>	<i>y</i>	<i>z</i>	U_{eq}^a
O1	0.2758(2)	0.3256(1)	0.3960(2)	0.0901(6)
O2	0.0808(1)	0.2848(1)	0.0905(1)	0.0676(5)
N1	0.1886(1)	0.4538(2)	0.2061(2)	0.0545(4)
C1	0.1334(1)	0.4641(1)	0.0771(2)	0.0515(5)
C2	0.1319(1)	0.5575(2)	0.0069(2)	0.0546(5)
C3	0.0796(1)	0.5596(2)	-0.1198(2)	0.0559(5)
C4	0.0271(1)	0.4674(2)	-0.1817(2)	0.0506(5)
C5	0.0277(1)	0.3732(2)	-0.1116(2)	0.0539(5)
C6	0.0789(1)	0.3718(2)	0.0159(2)	0.0523(5)
C7	0.0177(2)	0.1983(2)	0.0342(3)	0.0770(7)
C8	0.2176(2)	0.5414(2)	0.2771(2)	0.0560(5)
C9	0.2744(1)	0.5291(2)	0.4094(2)	0.0554(5)
C10	0.3009(1)	0.4214(2)	0.4652(2)	0.0641(6)
C11	0.3516(2)	0.4131(3)	0.5934(2)	0.0792(7)
C12	0.3758(2)	0.5092(3)	0.6653(3)	0.0797(7)
C13	0.3508(2)	0.6157(3)	0.6125(2)	0.0796(7)
C14	0.3011(2)	0.6254(2)	0.4860(2)	0.0701(6)
H1	0.234(2)	0.347(3)	0.314(3)	0.120(1)

H2	0.169(1)	0.620(2)	0.048(2)	0.054(5)
H3	0.083(2)	0.625(2)	-0.167(2)	0.081(7)
H5	-0.011(1)	0.309(1)	-0.158(2)	0.048(5)
H7A	-0.042(2)	0.232(2)	-0.012(3)	0.092(8)
H7B	0.021(2)	0.150(2)	-0.030(3)	0.091(8)
H7C	0.024(2)	0.149(2)	0.098(3)	0.092(8)
H8	0.198(1)	0.621(2)	0.246(2)	0.079(7)
H11	0.368(2)	0.340(3)	0.627(3)	0.097(9)
H12	0.409(2)	0.502(2)	0.752(3)	0.078(7)
H13	0.372(2)	0.681(3)	0.668(3)	0.104(9)
H14	0.279(2)	0.698(2)	0.446(2)	0.076(7)

^a U_{eq} is defined as one third of the trace of the orthogonalized U_{ij} tensor.

Table 6.4 Anisotropic displacement parameters.

<i>Atom</i>	U_{11}	U_{22}	U_{33}	U_{23}	U_{13}	U_{12}
O1	0.115(2)	0.058(1)	0.076(1)	0.0007(8)	0.033(1)	0.019(1)
O2	0.086(1)	0.054(1)	0.061(1)	0.007(1)	0.036(1)	-0.007(1)
N1	0.058(1)	0.054(1)	0.055(1)	-0.002(1)	0.031(1)	0.0008(7)
C1	0.055(1)	0.050(1)	0.055(1)	-0.001(1)	0.032(1)	0.004(1)
C2	0.063(1)	0.049(1)	0.059(1)	-0.006(1)	0.035(1)	-0.006(1)
C3	0.069(1)	0.048(1)	0.060(1)	0.001(1)	0.039(1)	-0.003(1)
C4	0.057(1)	0.047(1)	0.056(1)	0.0003(1)	0.035(1)	0.003(1)
C5	0.063(1)	0.045(1)	0.057(1)	-0.003(1)	0.032(1)	-0.003(1)
C6	0.062(1)	0.045(1)	0.057(1)	0.003(1)	0.035(1)	0.003(1)
C7	0.089(2)	0.060(1)	0.079(2)	0.012(1)	0.040(1)	-0.013(1)
C8	0.060(1)	0.054(1)	0.055(1)	-0.002(1)	0.030(1)	0.001(1)
C9	0.053(1)	0.057(1)	0.058(1)	-0.002(1)	0.023(1)	-0.003(1)

C10	0.063(1)	0.061(1)	0.066(1)	0.001(1)	0.030(1)	0.009(1)
C11	0.075(1)	0.082(2)	0.068(1)	0.014(1)	0.027(1)	0.019(1)
C12	0.065(1)	0.101(2)	0.056(1)	0.002(1)	0.018(1)	-0.0006(1)
C13	0.087(2)	0.084(2)	0.059(1)	-0.010(1)	0.029(1)	-0.018(1)
C14	0.083(2)	0.062(1)	0.060(1)	-0.006(1)	0.035(1)	-0.012(1)

Table 6.5 Bond distances (Å).

<i>Atoms</i>	<i>Bond distance</i>	<i>Atoms</i>	<i>Bond distance</i>
O1-C10	1.348(3)	C7-H7A	1.02(3)
O1-H1	0.95(4)	C7-H7B	1.00(3)
O2-C6	1.367(2)	C7-H7C	0.93(3)
O2-C7	1.420(3)	C8-C9	1.445(3)
N1-C8	1.284(3)	C8-H8	1.00(3)
N1-C1	1.407(3)	C9-C14	1.399(3)
C1-C2	1.393(3)	C9-C10	1.404(3)
C1-C6	1.403(3)	C10-C11	1.388(3)
C2-C3	1.373(3)	C11-C12	1.366(4)
C2-H2	0.95(2)	C11-H11	0.94(3)
C3-C4	1.389(3)	C12-C13	1.378(4)
C3-H3	0.98(3)	C12-H12	0.93(3)
C4-C5	1.404(3)	C13-C14	1.371(3)
C4-C4 ⁱ	1.476(4)	C13-H13	0.97(3)
C5-C6	1.379(3)	C14-H14	0.96(2)
C5-H5	0.99(2)		

Symmetry operation: (i) $[-x, y, -z - \frac{1}{2}]$

Table 6.6 Bond angles ($^{\circ}$).

<i>Atoms</i>	<i>Bond angles</i>	<i>Atoms</i>	<i>Bond angles</i>
C10-O1-H1	107(2)	O2-C7-H7A	111.6(1)
C6-O2-C7	117.2(2)	O2-C7-H7B	116.2(2)
C8-N1-C1	121.9(2)	H7A-C7-H7B	104.0(2)
C2-C1-C6	118.5(2)	O2-C7-H7C	106.9(2)
C2-C1-N1	124.2(2)	H7A-C7-H7C	111.0(2)
C6-C1-N1	117.2(2)	H7B-C7-H7C	107.0(2)
C3-C2-C1	121.3(2)	N1-C8-C9	121.1(2)
C3-C2-H2	119.9(1)	N1-C8-H8	122.4(1)
C1-C2-H2	118.7(1)	C9-C8-H8	116.4(1)
C2-C3-C4	120.6(2)	C14-C9-C10	118.2(2)
C2-C3-H3	119.4(1)	C14-C9-C8	120.0(2)
C4-C3-H3	119.9(1)	C10-C9-C8	121.7(2)
C3-C4-C5	118.5(2)	O1-C10-C11	119.5(2)
C3-C4-C4 ⁱ	120.9(1)	O1-C10-C9	120.7(2)
C5-C4-C4 ⁱ	120.6(1)	C11-C10-C9	119.7(2)
C6-C5-C4	121.1(2)	C12-C11-C10	120.3(3)
C6-C5-H5	122.0(1)	C12-C11-H11	122.4(2)
C4-C5-H5	116.9(1)	C10-C11-H11	117.3(2)
O2-C6-C5	124.3(2)	C11-C12-C13	120.9(3)
O2-C6-C1	115.7(2)	C11-C12-H12	119.4(1)
C5-C6-C1	119.9(2)	C13-C12-H12	119.6(1)
C14-C13-C12	119.5(3)	C13-C14-C9	121.3(2)
C14-C13-H13	123.3(2)	C13-C14-H14	121.9(1)
C12-C13-H13	117.1(2)	C9-C14-H14	116.6(1)

Symmetry operation: (i) $[-x, y, -z - \frac{1}{2}]$

Table 6.7 Torsion angles (°).

<i>Atoms</i>	<i>Torsion angles</i>	<i>Atoms</i>	<i>Torsion angles</i>
C8-N1-C1-C2	27.6(3)	N1-C8-C9-C14	-176.2(2)
C8-N1-C1-C6	-154.7(2)	C8-C9-C10-O1	1.9(3)
C6-C1-C2-C3	-1.2(3)	C14-C9-C10-C11	0.5(3)
N1-C1-C2-C3	176.5(2)	C8-C9-C10-C11	-176.4(2)
C1-C2-C3-C4	-0.6(3)	O1-C10-C11-C12	-178.4(2)
C2-C3-C4-C5	1.1(3)	C9-C10-C11-C12	0.0(4)
C2-C3-C4-C4 ⁱ	-177.9(2)	C10-C11-C12-C13	-0.2(5)
C3-C4-C5-C6	0.2(3)	C11-C12-C13-C14	-0.2(4)
C4 ⁱ -C4-C5-C6	179.2(2)	C12-C13-C14-C9	0.8(4)
C7-O2-C6-C5	-8.9(3)	C10-C9-C14-C13	-0.9(4)
C7-O2-C6-C1	170.9(2)	C8-C9-C14-C13	176.1(2)
C4-C5-C6-O2	177.8(2)	O1-C10-C9-C8	1.9(3)
C4-C5-C6-C1	-2.0(3)	C10-C9-C8-N1	0.7(3)
C2-C1-C6-O2	-177.4(2)	C9-C8-N1-C1	-179.9(2)
N1-C1-C6-O2	4.8(2)	N1-C1-C6-O2	4.8(2)
C2-C1-C6-C5	2.4(3)	C7-O2-C6-C5	-8.9(3)
N1-C1-C6-C5	-175.4(1)	C5-C4-C4 ⁱ -C5 ⁱ	-47.8(4)
C1-N1-C8-C9	-179.8(2)		

Symmetry operation: (i) $[-x, y, -z - \frac{1}{2}]$

Table 6.8 Hydrogen bonds (Å).

<i>D</i>	<i>H</i>	<i>A</i>	<i>D—H</i>	<i>H...A</i>	<i>D...A</i>	<i>D—H...A</i> (°)
O1	H1	N1	0.95(4)	1.71(4)	2.568(3)	147.9(3)
C2	H2	O1 ⁱⁱ	0.95(2)	2.57(2)	3.479(3)	159.8(18)

Symmetry operation: (ii) $[\frac{1}{2} - x, \frac{1}{2} + y, \frac{1}{2} - z]$

Table 6.9 Standard deviations of atoms from the planes (°).

Plane 1		Plane 2		Plane 3		Plane 4	
<i>Atoms</i>	<i>Deviations</i>	<i>Atoms</i>	<i>Deviations</i>	<i>Atoms</i>	<i>Deviations</i>	<i>Atoms</i>	<i>Deviations</i>
*C9	0.0006	*C1	-0.0106	*C1 ⁱ	-0.0106	*C9	-0.0037
*C8	-0.0006	*C2	0.0001	*C2 ⁱ	0.0001	*C10	0.0004
*N1	-0.0007	*C3	0.0082	*C3 ⁱ	0.0082	*C11	0.0021
*C1	0.0007	*C4	-0.0058	*C4 ⁱ	-0.0058	*C12	-0.0013
		*C5	-0.0049	*C5 ⁱ	-0.0049	*C13	-0.0021
		*C6	0.0130	*C6 ⁱ	0.0130	*C14	0.0046
		C7	0.2824			C7	-2.2028
		C8	0.3456			C8	-0.0818
		N1	-0.0907			N1	-0.1636
		O1	-0.8588			O1	-0.0298
		O2	0.0575			O2	-1.4046

* The atoms that constituted the planes.

Symmetry operation: (i) $[-x, y, -z - \frac{1}{2}]$

The equation of planes:

$$\text{Plane 1} \quad 17.87(1)x + 0.28(3)y + 7.64(1)z = 1.93(1)$$

$$\text{Plane 2} \quad -16.29(1)x + 4.90(1)y + 6.74(1)z = 0.63(1)$$

$$\text{Plane 3} \quad 16.29(1)x + 4.90(1)y - 6.74(1)z = 3.99(1)$$

$$\text{Plane 4} \quad 17.95(1)x + 0.72(1)y - 7.05(1)z = 2.42(1)$$

Table 6.10 Dihedral angles ($^{\circ}$).

<i>Planes</i>	<i>Dihedral angle</i>
1-2	26.2(1)
2-3	49.4(1)
3-4	21.3(1)
2-4	28.3(1)
1-4	3.9(1)

6.1.5 Molecular Graphics of $C_{28}H_{24}N_2O_4$ Crystal

Figure 6.2 shows the half-independent molecule that is in the asymmetric unit. An ORTEP3 diagram of the molecular structure of the title compound is shown in Figure 6.3, with the atom-numbering scheme. Figure 6.4 shows the packing of the title compound in the unit cell and the network of hydrogen bonding formed between C and O atoms. A space-filling (CPK) model with van der Waals radii assigned to each atom is given in Figure 6.5.

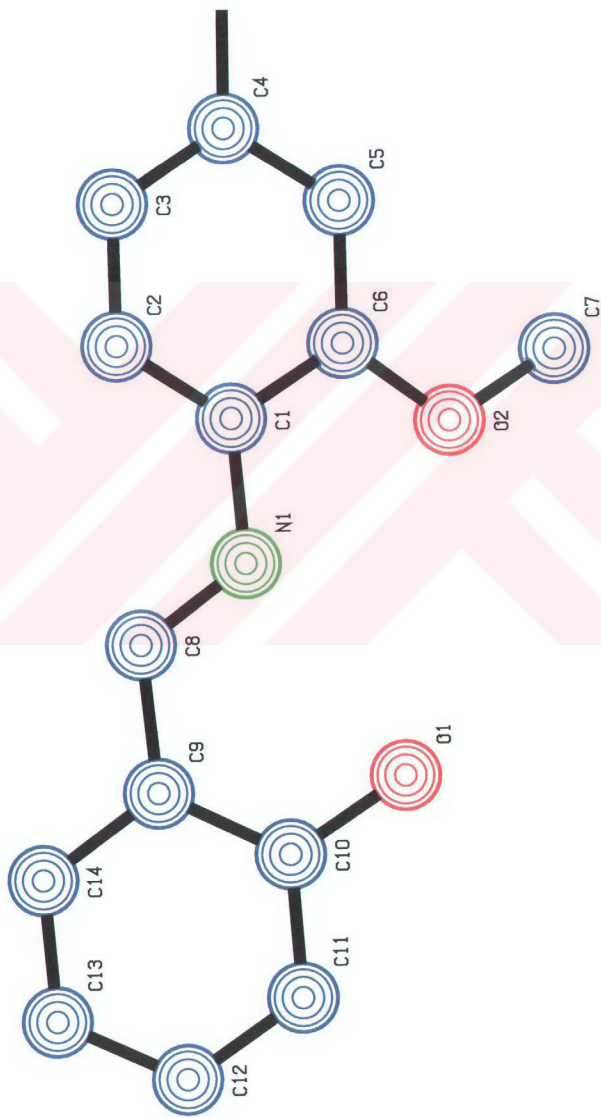


Figure 6.2 There is half-independent molecule in the asymmetric unit.

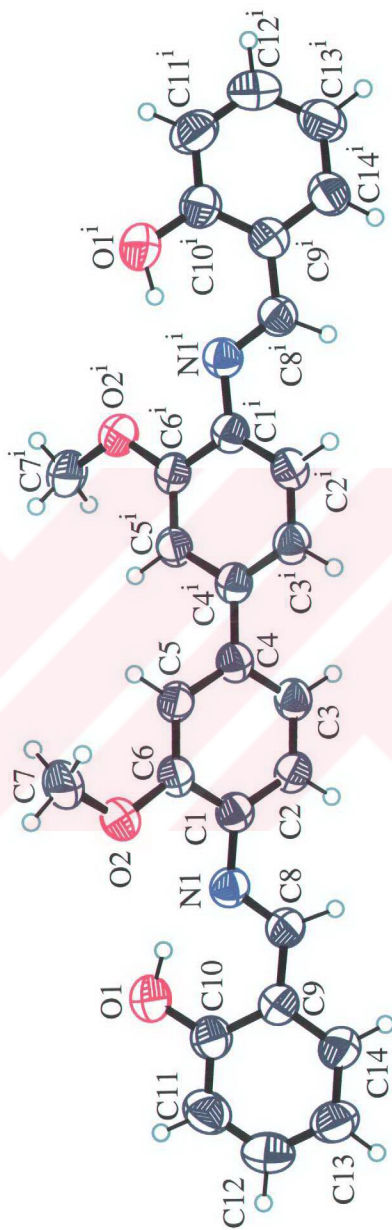


Figure 6.3. An ORTEP3 drawing of $C_{23}H_{24}N_2O_4$ showing the atomic numbering scheme. Displacement ellipsoids of non-H atoms are shown at the 50% probability level; H atoms are shown as small spheres of arbitrary size.

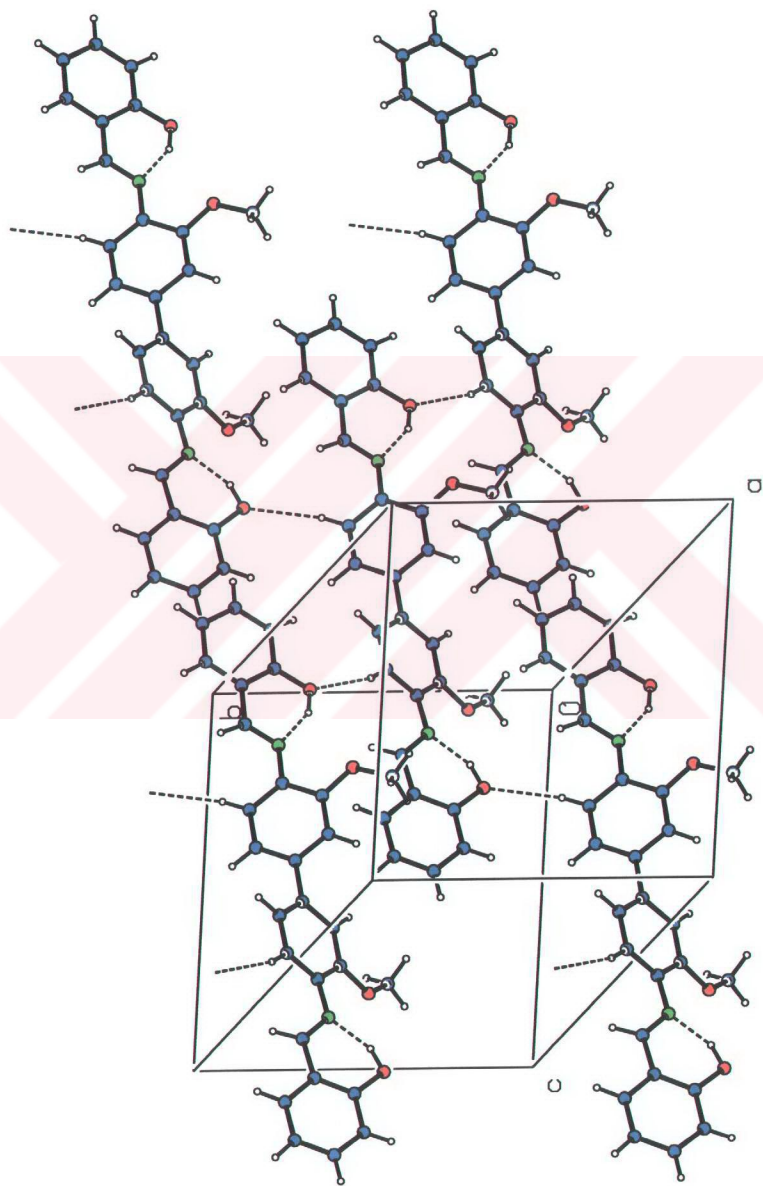


Figure 6.4 Unit cell contents with the hydrogen-bonding scheme indicated by dashed lines. [symmetry code: (ii) $\frac{1}{2}-x, \frac{1}{2}+y, \frac{1}{2}-z$]

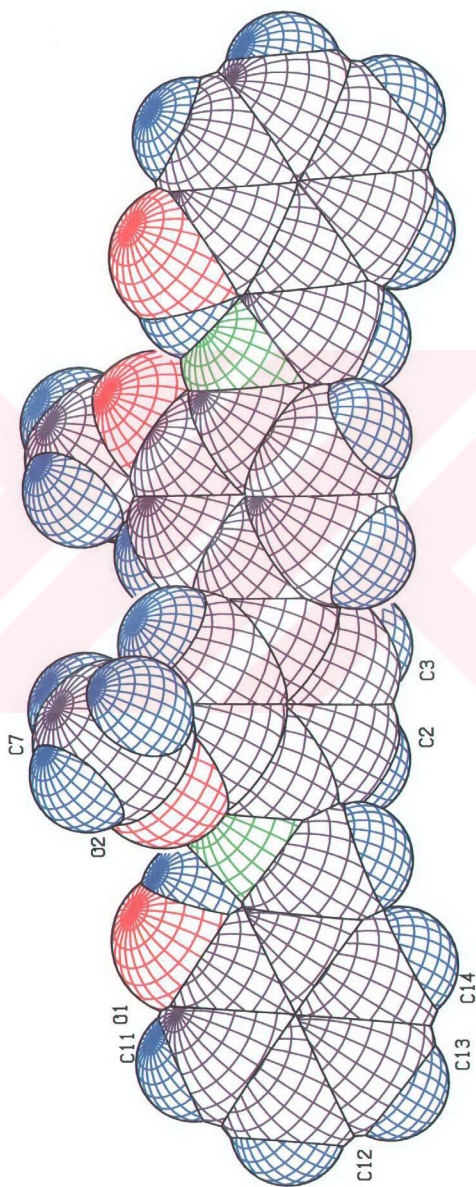


Figure 6.5 A CPK drawing of $C_{28}H_{24}N_2O_4$.

6.2 The Crystal of $C_{23}H_{32}N_4Se$

6.2.1 Synthesis of $C_{23}H_{32}N_4Se$ Crystal

The use of exobicyclic alkenes of the type **1** ($m=2$ or 3) as sources of *N*-heterocyclic carbene complexes of transition metals is well established (Lappert, 1988). However, larger rings, *i.e.* $m \geq 4$, have so far not been tackled. In an effort to fill the gap, we prepared **1c** ($R=p\text{-CH}_2\text{C}_6\text{H}_4\text{NMe}_2$, the R group was chosen so as to contain a quaternizable -NMe_2 functionality which would increase the water solubility) (Çetinkaya et al., In press). Under mild conditions **1c** reacted with Group VI elements to give cyclic chalcogeno ureas (eqn 1). This behavior is typical of reactive tetraaminoalkenes **1a** and **1b** (Çetinkaya et al., 1996; Winberg et al., 1965). In sharp contrast, **1c** is inert to electrophilic transition metal complexes such as $[\text{RuCl}_2(\eta^6\text{-arene})]_2$. This remarkable difference aroused our curiosity. Therefore, X-ray structure of the seleno urea **2c**, derived from the alkene **1c** was determined.

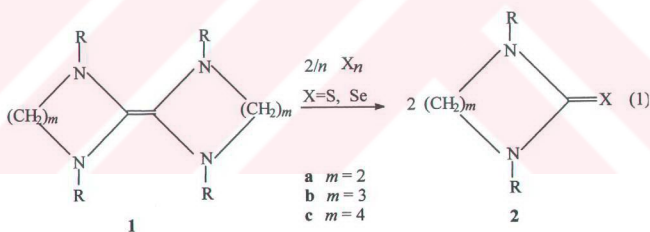


Figure 6.6 The chemical reaction of the title compound.

In a typical reaction, bis [1,3-bis(*p*-dimethylaminobenzyl)hexahydro-1,3-diazepine-2-ylidene], **1c** (0.886 g, 1.00 mmol) was heated with elemental selenium (0.200 g, 2.53 mmol) in refluxing toluene (20 mL) for 2 h. The resulting solution was cooled to room temperature and then filtered to remove the excess selenium. The volume of the filtrate was reduced to *ca* 10 mL and *n*-hexane (10 mL) was added.

Upon cooling the solution to $-20\text{ }^{\circ}\text{C}$ cream colored crystals of the title compound were obtained (0.54 g, 61%, m.p.= 141-142^o). All reactions were carried out under argon atmosphere with the use of Schlenk techniques. The solvents were dried and deoxygenated by standard procedures. Spectroscopic and analytical data of the compound is as follows:

^1H NMR (CDCl_3): δ 1.34 (br, 4H, $\text{NCH}_2\text{CH}_2\text{CH}_2\text{N}$), 2.92 (s, 12 H, $\text{CH}_2\text{C}_6\text{H}_4\text{N}(\text{CH}_3)_2$), 3.28 (br, 4H, $\text{NCH}_2\text{CH}_2\text{CH}_2\text{CH}_2\text{N}$), 5.07 (s, $\text{CH}_2\text{C}_6\text{H}_4\text{NMe}_2$), 6.67 (d, 4H, $\text{CH}_2\text{C}_6\text{H}_4\text{NMe}_2$, $J = 8.6$ Hz), 7.28 (d, 4H, $\text{CH}_2\text{C}_6\text{H}_4\text{NMe}_2$, $J = 8.6$ Hz); $^{13}\text{C}\{^1\text{H}\}$ NMR (CDCl_3) δ 24.30 ($\text{NCH}_2\text{CH}_2\text{CH}_2\text{CH}_2\text{N}$), 40.50 ($\text{NCH}_2\text{CH}_2\text{CH}_2\text{CH}_2\text{N}$), 50.41 ($\text{C}_6\text{H}_4\text{N}(\text{CH}_3)_2$), 61.5 ($\text{CH}_2\text{C}_6\text{H}_4\text{NMe}_2$), 112.4, 125.0, 129.6, 150.0 ($\text{CH}_2\text{C}_6\text{H}_4\text{NMe}_2$), 192.8 (C=Se). Anal. called for $\text{C}_{23}\text{H}_{32}\text{N}_4\text{Se}$: C, 62.29; H, 7.27; N, 12.63; found: C, 60.15; H, 7.30; N, 12.39 (Çetinkaya et al., In press).

6.2.2 Data Collection of $\text{C}_{23}\text{H}_{32}\text{N}_4\text{Se}$ Crystal

The suitable crystals were selected from the synthesized crystals by using stereomicroscope and polarization microscope. Before starting data collection, a sample of size $0.09 \times 0.40 \times 0.40\text{ mm}^3$ was selected for the crystallographic study.

The diffraction measurements were performed at room temperature (293K) on an Enraf-Nonius CAD-4 diffractometer using graphite-monochromated MoK_α radiation. Orientation matrix and unit cell parameters were obtained from the setting angles of 25 reflections at medium θ ($1.48^\circ < \theta < 26.34^\circ$). The systematic absences and intensity symmetries indicated the monoclinic $Pbca$ space group. A total of 4617 intensities with $\theta_{\text{max}}=26.34^\circ$ were collected in the $w/2\theta$ scan mode, as suggested by peak-shape analyses. The crystal and equipment stabilities were checked by the intensities of three standard reflections monitored every 120 minutes. No significant intensity decay was observed (~2%). The intensities were corrected for Lorentz and Polarization factors, but not for absorption effect ($\mu = 1.673\text{ mm}^{-1}$).

6.2.3 Structure Solution & Refinement of $C_{23}H_{32}N_4Se$ Crystal

The structure was solved by direct methods using *SHELXS-97* for 2626 reflections with $I)2\sigma(I)$. FOM values that used in phase determination are given in Table 6.11. Since the $\langle |E^2 - 1| \rangle$ value is 0.961, structure is centrosymmetric. The refinement was carried out by full-matrix least squares. The non-hydrogen atoms were refined anisotropically. The structure was refined to $R = 0.061$ for the observed reflections and $R = 0.112$ for all data. The maximum and minimum peaks, observed in the final $\Delta\rho$ map, were 0.492 and $-0.548 \text{ e}\text{\AA}^{-3}$, respectively. The scattering factors were taken from *SHELXL-97*. H atoms were added at calculated positions and refined using a riding model with $U_{iso}(H) = xU_{eq}(\text{parent atom})$, where $x = 1.5$ for methyl and 1.2 for others. The U_{iso} values for H atoms are in the range 0.084-0.265.

Table 6.11 FOM values for $C_{23}H_{32}N_4Se$.

Set Code	R_α	NQUAL	MABS	CFOM
414597	0.071	-0.896	1.333	0.071

6.2.4 Experimental Results for $C_{23}H_{32}N_4Se$ Crystal

Table 6.12 Crystallographic data for the title compound.

Crystal Data	
Chemical formula	$C_{23}H_{32}N_4Se$
Color/shape	cream/needle
Formula weight (<i>a.m.u.</i>)	443.49
Space group	Pbca
Crystal system	Orthorhombic

a, b, c (Å)	10.996(1), 14.946(1), 27.565(5)
α, β, γ (°)	90, 90, 90
Cell volume (Å ³)	4530.2(9)
Formula unit cell (Z)	8
D_x (g/cm ³)	1.300
F_{000}	1856
Absorption coefficient μ (mm ⁻¹)	1.673
Crystal size (mm ³)	0.09 × 0.40 × 0.40

Data Collection	
Diffractometer	Enraf-Nonius CAD-4
Temperature (K)	293(2)
Scan type	$\omega/2\theta$
Radiation/Wavelength λ (Å)	$MoK_{\alpha}/0.71069$
Reflections measured	4617
Independent/observed reflections	4617/2626
Range of h, k, l	0→13, 0→18, 0→34
Standard reflections	3
Standards interval time (min)	120
Standards decay %	2

Refinement	
Data/Restraints/Parameters	2626/0/291
Extinction Coefficient	0.0029(6)

Final R indices $[I]2\sigma(I)$	$R_1 = 0.061, wR_2 = 0.180$
R indices (all data)	$R_1 = 0.112, wR_2 = 0.212$
GOF (onF^2)	1.070
$\Delta\rho_{\min}/\Delta\rho_{\max}$ ($e/\text{\AA}^3$)	-0.548/0.492
$(\Delta/\sigma)_{\max}$	0.005
Weighting function	$w = [\sigma^2(F_{obs}^2) + (0.1185P)^2 + 0.1331P]^{-1}$ $P = \frac{1}{3}(F_{obs}^2 + 2F_{cal}^2)$

Table 6.13 Atomic coordinates and equivalent isotropic thermal parameters (\AA^2).

Atom	x	y	z	U_{eq}^a
Se1	0.76058(4)	0.13507(4)	0.67879(2)	0.0919(3)
N1	0.8764(4)	0.2964(3)	0.7023(1)	0.111(2)
N2	1.0954(5)	0.3203(4)	0.4830(2)	0.127(2)
N3	0.8748(4)	0.1931(3)	0.7642(1)	0.097(1)
N4	0.5726(5)	-0.0245(3)	0.9272(2)	0.119(2)
C1	0.8448(4)	0.2151(3)	0.7182(1)	0.085(1)
*C2A	0.9141(19)	0.2403(10)	0.8042(5)	0.108(5)
#C2B	0.8677(12)	0.2748(12)	0.8015(5)	0.070(3)
*C3A	0.9906(10)	0.3111(6)	0.8068(3)	0.086(3)
#C3B	0.8792(15)	0.3349(10)	0.7971(4)	0.102(5)
#C4A	1.0375(12)	0.3323(13)	0.7561(7)	0.118(6)
*C4B	0.9672(14)	0.3886(8)	0.7655(5)	0.103(4)
*C5A	1.0074(11)	0.3272(8)	0.7240(5)	0.081(3)
#C5B	0.9437(16)	0.3705(10)	0.7244(6)	0.100(4)

#C5B	0.9437(16)	0.3705(10)	0.7244(6)	0.100(4)
C6	0.8221(6)	0.3376(4)	0.6596(2)	0.106(2)
C7	0.9015(4)	0.3341(3)	0.6148(2)	0.082(1)
C8	0.9880(5)	0.2703(3)	0.6071(2)	0.096(1)
C9	1.0538(5)	0.2652(3)	0.5644(2)	0.098(1)
C10	1.0327(5)	0.3235(3)	0.5268(2)	0.092(1)
C11	0.9446(5)	0.3891(3)	0.5343(2)	0.091(1)
C12	0.8827(5)	0.3945(3)	0.5781(2)	0.090(1)
C13	1.1863(7)	0.2514(5)	0.4765(3)	0.157(3)
C14	1.0459(10)	0.3577(5)	0.4398(3)	0.177(4)
C15	0.8948(4)	0.1015(4)	0.7789(2)	0.096(1)
C16	0.8088(4)	0.0678(3)	0.8171(2)	0.078(1)
C17	0.8518(4)	0.0203(3)	0.8570(2)	0.091(1)
C18	0.7753(4)	-0.0119(4)	0.8926(2)	0.095(2)
C19	0.6495(4)	0.0041(3)	0.8903(2)	0.086(1)
C20	0.6069(4)	0.0516(3)	0.8504(2)	0.082(1)
C21	0.6847(4)	0.0819(3)	0.8148(2)	0.080(1)
C22	0.4444(6)	-0.0135(5)	0.9211(2)	0.131(2)
C23	0.6135(7)	-0.094(5)	0.9583(3)	0.155(3)
H2A1	0.8402	0.2603	0.8201	0.129
H2A2	0.9493	0.1957	0.8255	0.129
H2B1	0.7873	0.2701	0.8157	0.084
H2B2	0.9240	0.2588	0.8272	0.084
H3A1	1.0582	0.2971	0.8281	0.103
H3A2	0.9481	0.3626	0.8200	0.103
H3B1	0.8931	0.3576	0.8296	0.123
H3B2	0.7996	0.3569	0.7878	0.123
H4A1	1.0599	0.3949	0.7584	0.142
H4A2	1.1141	0.3001	0.7548	0.142
H4B1	0.9569	0.4522	0.7712	0.124
H4B2	1.0507	0.3725	0.7729	0.124
H5A1	1.0653	0.2882	0.7079	0.097

H5A2	1.0206	0.3860	0.7100	0.097
H5B1	1.0222	0.3691	0.7084	0.120
H5B2	0.9033	0.4237	0.7121	0.120
H6A	0.8040	0.3997	0.6670	0.127
H6B	0.7458	0.3078	0.6527	0.127
H8	1.0033	0.2286	0.6314	0.116
H9	1.1134	0.2215	0.5611	0.118
H11	0.9271	0.4297	0.5097	0.110
H12	0.8268	0.4404	0.5827	0.108
H13A	1.2228	0.2575	0.4450	0.236
H13B	1.1487	0.1936	0.4791	0.236
H13C	1.2478	0.2573	0.5010	0.236
H14A	1.1023	0.3500	0.4136	0.265
H14B	1.0308	0.4204	0.4447	0.265
H14C	0.9708	0.3281	0.4321	0.265
H15A	0.9773	0.0961	0.7910	0.115
H15B	0.8879	0.0634	0.7505	0.115
H17	0.9349	0.0100	0.8598	0.109
H18	0.8072	-0.0445	0.9183	0.114
H20	0.5241	0.0632	0.8477	0.099
H21	0.6528	0.1128	0.7884	0.096
H22A	0.4030	-0.0357	0.9493	0.196
H22B	0.4181	-0.0463	0.8930	0.196
H22C	0.4260	0.0487	0.9168	0.196
H23A	0.5519	-0.1076	0.9820	0.233
H23B	0.6868	-0.0765	0.9745	0.233
H23C	0.6292	-0.1475	0.9394	0.233

^a U_{eq} is defined as one third of the trace of the orthogonalized U_y tensor.

* Site occupancy factor 0.53

Site occupancy factor 0.47

Table 6.14 Anisotropic displacement parameters .

<i>Atom</i>	U_{11}	U_{22}	U_{33}	U_{23}	U_{13}	U_{12}
Se1	0.0802(4)	0.1154(5)	0.0800(4)	-0.0100(3)	-0.0025(2)	-0.0177(3)
N1	0.141(4)	0.127(3)	0.066(2)	-0.060(3)	-0.003(2)	0.009(2)
N2	0.127(4)	0.158(5)	0.096(3)	-0.004(3)	0.039(3)	-0.006(3)
N3	0.113(3)	0.112(3)	0.065(2)	-0.044(2)	-0.005(2)	0.000(2)
N4	0.109(3)	0.130(4)	0.120(4)	-0.010(3)	0.007(3)	0.053(3)
C1	0.083(3)	0.110(3)	0.062(2)	-0.022(2)	0.003(2)	-0.002(2)
C2A	0.18(2)	0.07(1)	0.07(1)	0.01(1)	-0.01(1)	-0.01(1)
C2B	0.087(7)	0.060(8)	0.064(6)	-0.004(6)	0.013(5)	-0.018(7)
C3A	0.085(6)	0.086(6)	0.088(6)	-0.007(5)	-0.010(5)	-0.017(5)
C3B	0.14(1)	0.08(1)	0.09(1)	-0.01(1)	0.02(1)	-0.03(1)
C4A	0.073(7)	0.166(15)	0.115(13)	-0.027(8)	-0.025(8)	0.018(11)
C4B	0.11(1)	0.10(1)	0.09(1)	-0.03(1)	0.01(1)	-0.02(1)
C5A	0.072(6)	0.081(7)	0.089(8)	-0.010(5)	-0.004(5)	0.011(6)
C5B	0.11(1)	0.09(1)	0.11(1)	-0.03(1)	0.00(1)	0.02(1)
C6	0.139(5)	0.101(4)	0.076(3)	-0.016(3)	0.022(3)	0.002(3)
C7	0.088(3)	0.087(3)	0.070(3)	-0.011(2)	0.005(2)	0.009(2)
C8	0.105(3)	0.098(3)	0.087(3)	-0.005(3)	0.002(3)	0.019(3)
C9	0.094(3)	0.093(3)	0.109(4)	0.003(3)	0.007(3)	0.002(3)
C10	0.098(3)	0.091(3)	0.086(3)	-0.014(3)	0.018(3)	-0.006(3)
C11	0.098(3)	0.105(3)	0.071(3)	-0.007(3)	0.013(2)	0.013(2)
C12	0.090(3)	0.088(3)	0.091(3)	-0.001(2)	0.011(3)	0.009(3)
C13	0.140(6)	0.149(6)	0.184(7)	-0.007(5)	0.068(5)	-0.051(5)
C14	0.29(1)	0.14(1)	0.100(0)	0.00(1)	0.07(1)	0.01(0)
C15	0.075(3)	0.130(4)	0.083(3)	-0.005(3)	-0.008(2)	0.003(3)
C16	0.072(2)	0.087(3)	0.076(3)	0.004(2)	-0.006(2)	0.008(2)
C17	0.073(3)	0.107(3)	0.093(3)	0.011(2)	-0.009(2)	0.011(3)
C18	0.092(3)	0.098(4)	0.095(3)	0.012(3)	-0.021(3)	0.025(3)

C19	0.089(3)	0.076(3)	0.093(3)	-0.005(2)	-0.006(3)	0.019(2)
C20	0.071(2)	0.081(3)	0.096(3)	-0.001(2)	-0.001(2)	0.020(2)
C21	0.077(3)	0.079(3)	0.085(3)	0.005(2)	-0.008(2)	0.014(2)
C22	0.110(4)	0.164(6)	0.118(5)	-0.020(4)	0.022(4)	0.024(4)
C23	0.168(7)	0.177(6)	0.121(5)	-0.014(5)	0.002(5)	0.069(5)

Table 6.15 Bond distances (Å).

<i>Atoms</i>	<i>Bond distance</i>	<i>Atoms</i>	<i>Bond distance</i>
Se1-C1	1.862(5)	N3-C1	1.351(6)
N3-C15	1.444(8)	N3-C2A	1.38(2)
C21-C20	1.380(7)	C21-C16	1.382(7)
C19-C20	1.390(7)	C19-C18	1.405(7)
C19-N4	1.388(7)	C12-C11	1.388(7)
C12-C7	1.372(7)	C16-C17	1.392(7)
C16-C15	1.503(7)	C1-N1	1.338(7)
C18-C17	1.378(8)	C11-C10	1.394(8)
N1-C6	1.456(7)	N1-C5B	1.46(2)
N4-C22	1.429(8)	N4-C23	1.43(1)
C7-C8	1.363(8)	C7-C6	1.515(8)
C8-C9	1.383(8)	C10-C9	1.375(8)
C10-N2	1.391(8)	C13-N2	1.45(1)
N2-C14	1.42(1)	C5A-C5B	0.95(3)
C5A-C4A	0.95(3)	C5A-C4B	1.53(2)
C5B-C4A	1.47(3)	C5B-C4B	1.19(3)
C2A-C2B	0.73(3)	C2A-C3A	1.35(3)
C2A-C3B	1.48(3)	C2B-C3A	1.46(2)
C2B-C3B	0.92(3)	C4A-C4B	1.17(3)
C4A-C3A	1.52(3)	C4B-C3B	1.53(3)
C3A-C3B	1.30(2)		

Table 6.16 Bond angles ($^{\circ}$).

<i>Atoms</i>	<i>Bond angles</i>	<i>Atoms</i>	<i>Bond angles</i>
C1-N3-C15	122.0(5)	C1-N3-C2A	134.6(8)
C15-N3-C2A	102.4(8)	C20-C21-C16	122.0(5)
C20-C19-C18	116.9(5)	C20-C19-N4	122.1(5)
C18-C19-N4	121.0(5)	C11-C12-C7	121.9(5)
C21-C20-C19	121.5(5)	C21-C16-C17	116.7(5)
C21-C16-C15	122.5(5)	C17-C16-C15	120.8(5)
Se1-C1-N3	120.8(4)	Se1-C1-N1	121.5(4)
N3-C1-N1	117.7(5)	C19-C18-C17	120.7(5)
C12-C11-C10	120.7(5)	C1-N1-C6	122.8(5)
C1-N1-C5B	133.1(7)	C6-N1-C5B	102.8(8)
C16-C17-C18	122.2(5)	C19-N4-C22	118.7(5)
C19-N4-C23	118.3(5)	C22-N4-C23	117.7(6)
N3-C15-C16	114.7(5)	C12-C7-C8	116.8(5)
C12-C7-C6	119.5(5)	C8-C7-C6	123.6(5)
C7-C8-C9	122.4(5)	C11-C10-C9	116.8(5)
C11-C10-N2	119.8(5)	C9-C10-N2	123.3(5)
C8-C9-C10	121.3(5)	N1-C6-C7	114.1(5)
C10-N2-C13	118.4(6)	C10-N2-C14	121.4(6)
C13-N2-C14	116.2(6)	C5B-C5A-C4A	101.0(19)
C5B-C5A-C4B	51.2(13)	C4A-C5A-C4B	49.8(14)
N1-C5B-C5A	81.5(13)	N1-C5B-C4A	107.9(13)
N1-C5B-C4B	132.4(14)	C5A-C5B-C4A	39.4(13)
C5A-C5B-C4B	90.3(17)	C4A-C5B-C4B	50.9(12)
N3-C2A-C2B	93.6(20)	N3-C2A-C3B	107.7(13)
C2B-C2A-C3A	83.6(19)	C2B-C2A-C3B	29.4(16)
C3A-C2A-C3B	54.6(10)	C2A-C2B-C3A	66.8(19)
C2A-C2B-C3B	127.6(26)	C3A-C2B-C3B	61.4(14)

C5A-C4A-C5B	39.6(12)	C5A-C4A-C4B	91.9(17)
C5A-C4A-C3A	136.2(16)	C5B-C4A-C4B	52.3(12)
C5B-C4A-C3A	112.9(12)	C4B-C4A-C3A	73.9(12)
C5A-C4B-C5B	38.5(10)	C5A-C4B-C4A	38.3(11)
C5A-C4B-C3B	107.1(11)	C5B-C4B-C4A	76.8(15)
C5B-C4B-C3B	106.6(14)	C4A-C4B-C3B	99.6(14)
C2A-C3A-C2B	29.6(11)	C2A-C3A-C4A	108.9(12)
C2A-C3A-C3B	67.5(12)	C2B-C3A-C4A	107.3(10)
C2B-C3A-C3B	38.1(10)	C4A-C3A-C3B	94.2(10)
C2A-C3B-C2B	23.0(13)	C2A-C3B-C4B	114.4(14)
C2A-C3B-C3A	57.9(11)	C2B-C3B-C4B	132.7(17)
C2B-C3B-C3A	80.5(15)	C4B-C3B-C3A	70.4(11)

Table 6.17 Torsion angles ($^{\circ}$).

<i>Atoms</i>	<i>Torsion angles</i>	<i>Atoms</i>	<i>Torsion angles</i>
C16-C21-C20-C19	-0.81 (69)	N4-C19-C20-C21	178.07 (48)
C18-C19-C20-C21	-0.21 (68)	C20-C21-C16-C17	0.65 (64)
C20-C21-C16-C15	-179.13 (47)	C2A-N3-C1-N1	13.91 (1.47)
C15-N3-C1-N1	-152.59 (46)	C2B-N3-C1-N1	35.39 (77)
C2A-N3-C1-Se1	-165.34 (1.31)	C15-N3-C1-Se1	28.16 (61)
C2B-N3-C1-Se1	-143.86 (59)	N4-C19-C18-C17	-176.93 (49)
C20-C19-C18-C17	1.36 (74)	C7-C12-C11-C10	-2.71 (78)
N3-C1-N1-C6	-162.50 (50)	Se1-C1-N1-C6	16.74 (70)
N3-C1-N1-C5B	2.39 (1.35)	Se1-C1-N1-C5B	-178.37 (1.14)
N3-C1-N1-C5A	36.42 (73)	Se1-C1-N1-C5A	-144.34 (55)
C19-C18-C17-C16	-1.56 (81)	C21-C16-C17-C18	0.53 (71)
C15-C16-C17-C18	-179.69 (50)	C20-C19-N4-C22	7.25 (79)
C18-C19-N4-C22	-174.55 (54)	C20-C19-N4-C23	160.88 (57)

C18-C19-N4-C23	-0.92 (80)	C1-N3-C15-C16	-118.24 (48)
C2A-N3-C15-C16	71.57 (1.01)	C2B-N3-C15-C16	53.02 (78)
C21-C16-C15-N3	45.82 (62)	C17-C16-C15-N3	-133.95 (46)
C11-C12-C7-C8	2.70 (73)	C11-C12-C7-C6	-173.69 (49)
C12-C7-C8-C9	-0.51 (75)	C6-C7-C8-C9	175.71 (50)
C12-C11-C10-C9	0.42 (74)	C12-C11-C10-N2	-178.71 (48)
N2-C10-C9-C8	-179.18 (50)	C11-C10-C9-C8	1.72 (76)
C7-C8-C9-C10	-1.73 (82)	C1-N1-C6-C7	-102.34 (58)
C5B-N1-C6-C7	88.91 (89)	C5A-N1-C6-C7	56.67 (79)
C8-C7-C6-N1	26.16 (71)	C12-C7-C6-N1	-157.71 (45)
C9-C10-N2-C14	157.40 (62)	C11-C10-N2-C14	-23.53 (87)
C9-C10-N2-C13	0.87 (86)	C11-C10-N2-C13	179.94 (53)
C1-N1-C5A-C4A	-55.40 (2.82)	C6-N1-C5A-C4A	143.49 (2.55)
C5B-N1-C5A-C4A	79.90 (2.84)	C1-N1-C5B-C4B	-18.95 (3.48)
C6-N1-C5B-C4B	148.06 (2.59)	C5A-N1-C5B-C4B	-82.59 (2.56)
C1-N3-C2A-C3A	-37.27 (2.74)	C15-N3-C2A-C3A	131.04 (1.75)
C2B-N3-C2A-C3A	-84.67 (2.19)	C1-N3-C2B-C3B	-29.91 (2.34)
C2A-N3-C2B-C3B	115.08 (3.57)	C15-N3-C2B-C3B	158.20 (1.96)
N1-C5A-C4A-C3A	4.50 (5.04)	N1-C5B-C4B-C3B	-18.06 (3.48)
N3-C2A-C3A-C4A	-2.73 (2.27)	C5A-C4A-C3A-C2A	30.61 (3.67)
N3-C2B-C3B-C4B	-36.92 (3.51)	C5B-C4B-C3B-C2B	63.03 (3.28)

The equation of planes:

$$\text{Plane 1} \quad -0.21(7)x + 9.38(9)y + 21.4(2)z = 19.5(1)$$

$$\text{Plane 2} \quad 1.27(2)x + 12.78(1)y + 13.91(5)z = 13.26(4)$$

$$\text{Plane 3} \quad 7.68(1)x + 9.10(2)y + 10.32(4)z = 16.32(2)$$

$$\text{Plane 4} \quad 7.89(4)x + 10.41(6)y - 0.03(30)z = 11.9(1)$$

Table 6.18 Standard deviations of atoms from the planes (°).

Plane 1		Plane 2		Plane 3		Plane 4	
Atoms	Deviations	Atoms	Deviations	Atoms	Deviations	Atoms	Deviations
*N4	0.0000	*C17	0.0058	*C7	0.0134	*N2	0.0000
*C22	0.0000	*C18	-0.0088	*C8	-0.0063	*C13	0.0000
*C23	0.0000	*C19	0.0018	*C9	-0.0055	*C14	0.0000
		*C20	0.0031	*C10	-0.0097		
		*C21	0.0044	*C11	-0.0088		
		*C22	-0.0063	*C12	0.0169		

* The atoms that constituted the planes.

Table 6.19 Dihedral angles (°).

Planes	Dihedral angle
1-2	21.9(7)
2-3	37.7(2)
3-4	22.2(6)
2-4	47.3(5)
1-4	65.0(7)
1-3	48.7(5)

6.2.5 Molecular Graphics of $C_{23}H_{32}N_4Se$ Crystal

An ORTEP3 diagram of the molecular structure of $C_{23}H_{32}N_4Se$ is shown in Figure 6.7, with the atom-numbering scheme. Figure 6.8 shows the packing of the $C_{23}H_{32}N_4Se$ in the unit cell. A space-filling (CPK) model with van der Waals radii assigned to each atom is given in Figure 6.9.

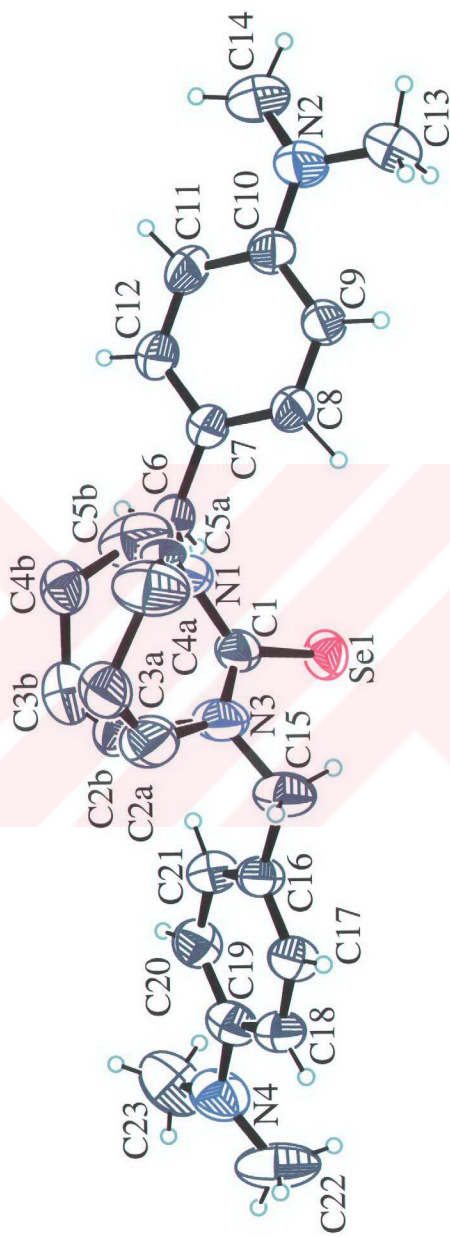


Figure 6.7 An ORTEP3 view of the $C_{23}H_{32}N_4Se$ with the non-H atoms shown with displacement ellipsoids drawn at the 30% probability level. H atoms in diazepine ring are omitted for clarity and the others are shown as small spheres of arbitrary size.

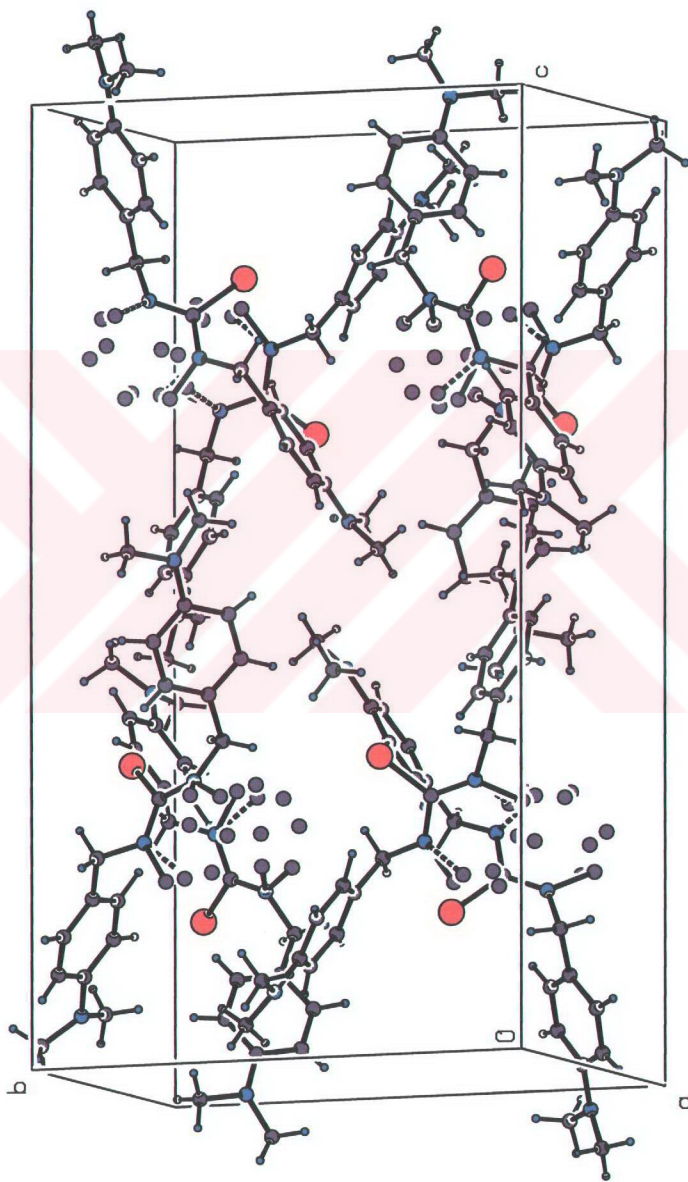


Figure 6.8 Unit cell packing diagram of $C_{31}H_{32}N_4Se$.

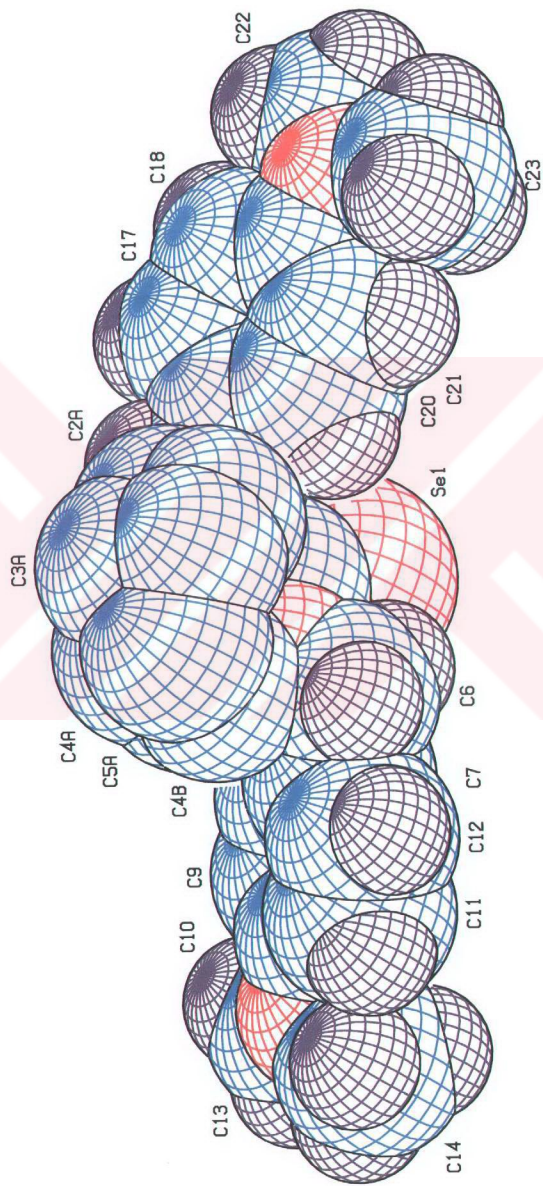


Figure 6.9 A CPK drawing of $C_{23}H_{32}N_4Se$.

CHAPTER SEVEN

CONCLUSION

7.1 Conclusion

In this study, molecular and crystal structures of ‘3,3’-dimethoxybenzidine(2-hydroxybenzal)diimine’, $C_{28}H_{24}N_2O_4$, and ‘hexahydrobis[(1,3-*p*-dimethylamino-benzyl)-1,3-diazepine-2-selenone’, $C_{23}H_{32}N_4Se$, have been determined by single crystal X-ray diffraction technique.

There is half-independent molecule of $C_{28}H_{24}N_2O_4$ in the asymmetric unit that is shown in Figure 7.2. The molecule has a two-fold symmetry on the mid point of the C(4)-C(4)ⁱ bond. The C=N imine bond and C-N-C bond angle can be compared with 1.284(3)Å and 121.9(2)° values in 3-methoxyphenyl-salicylaldimine (Elmalı et al., 1999) and N-(2-methy-5-chlorophenyl)salicylaldimine (Elmalı&Elerman, 1998). The C(4)-C(4)ⁱ bond length, 1.476(4)Å is within the range of a single C-C bond length. The C6-O2 and O2-C7 distances of 1.367(2)Å, 1.420(3)Å and the C6-O2-C7 angle of 117.2(2)° are consistent with the similar compounds which have the values 1.372(2)Å, 1.415(2)Å and 117.9(1)° in 3-methoxyphenyl-salicylaldimine (Elmalı et al., 1999), 1.363(2)Å, 1.417(2)Å and 117.5(2)°, 1.360(2)Å, 1.415(2)Å and 117.6(2)° in N-2-[3’-(methoxysalicylideneimino)benzyl]-3’’-methoxysalicylideneimine (Dey et al., 2001). The bond lengths and angles in the molecule are comparable to the analogous values in *ortho*-hydroxy Schiff base compounds (Fernandez et al., 2001; Filarowski et al., 1999).

Both six-membered rings are planar with a maximum deviation of 0.013(2)Å. The methoxy O, C and hydroxy O atoms are slightly away from the planes of their respective phenyl rings; the values are 0.058(3)Å, 0.0283(4)Å and 0.030(4)Å, respectively. The imine moiety makes dihedral angles of 3.9(1)° and 26.2(1)° with the hydroxyphenyl and methoxyphenyl ring planes, respectively. The dihedral angle between hydroxyphenyl and methoxyphenyl ring planes is 28.3(1)°. In addition, the dihedral angle between two methoxyphenyl ring planes is 49.4(1)°.

2-hydroxy Schiff base ligands are of interest mainly due to the existence of O-H...N and O...H-N type hydrogen bonds and tautomerism between phenol-imine and keto-imine forms. In these compounds, short hydrogen bonds were observed between the 2-hydroxy group and imine nitrogen (Nazir et al., 2000; Elmalı et al., 1998). The title compound crystallizes in the solid state into the phenol-imine tautomeric form with O-H distances of 0.95(4)Å. There is a strong intramolecular hydrogen bond of distance 2.568(3)Å between hydroxy oxygen atom and imine nitrogen atom, while H...N distance is 1.71(4)Å; the value for the O-H...N angle is 147.9(3)°. C-H...X hydrogen bonds have been postulated to stabilize the geometries of many organic compounds in the solid state (Kazak et al., 2000, Aygün et al., 1998). The crystal structure is stabilized by one weak intermolecular hydrogen bond between C(2)...O(1)ⁱⁱ [C(2)...O(1)ⁱⁱ 3.479(3)Å, C(2)-H(2) 0.95(2)Å, H(2)... O(1)ⁱⁱ 2.57(2)Å, C(2)-H(2)... O(1)ⁱⁱ 159.8(18)°; symmetry code: (ii) ½-x, ½+y, ½-z] and also by van der Waals interactions.

In $C_{23}H_{32}N_4Se$, the diazepine ring proved to be disordered over two orientations. The site-occupancy of the major disordered component refined to the value of 0.53(1). The relatively high R-values are related to the weak scattering that is most probably a consequence of the disorder in the diazepine ring of $C_{23}H_{32}N_4Se$. The displacement parameters of atoms C2, C3, C4 and C5 of the diazepine ring are quite high, resulting in unusual bond lengths involving these atoms. The distances between these partially populated sites of the C2A-C2B, C3A-C3B, C4A-C4B and C5A-C5B are 0.73(3), 1.30(2), 1.17(3) and 0.95(3)Å, respectively. The other bond lengths and angles are in agreement with those in the literature. The both partially populated sites

of the diazepine ring are nonplanar. The dihedral angle between the two phenyl rings is $37.7(2)^\circ$ and each of the dimethylamino groups is tilted from the phenyl ring to which it is attached. The first dimethylamino group (C13-N2-C14) is tilted $22.2(6)^\circ$ from the plane of phenyl ring while the second dimethylamino group (C22-N4-C23) is tilted $21.9(7)^\circ$ from the plane of phenyl ring. There are three intramolecular interactions: two of them are C-H...Se type and the other one is C-H...N type [C6...Se1 3.146(6)Å, C6-H6B 0.970(7)Å and C6-H6B...Se1 109.6(3)°; C15...Se1 3.168(5)Å, C15-H15B 0.970(5)Å and C15-H15B...Se1 113.9(3)°; C8...N1 2.924(6)Å, C8-H8 0.930(5)Å and C8-H8...N1 100.6(3)°]. The molecules in the crystal are packed by normal van der Waals distances.



REFERENCES

- Aygün, M., Işık, Ş., Öcal, N., Tahir, M. N., Kaban, Ş. & Büyüküngör, O. (1998). Thiophene-2-carbaldehyde N-(2,4-Dinitrophenyl)-N-methylhydrazone. Acta Crystallographica, C54, 527-529.
- Aygün, M. (1997). Tek Kristal X-Işınları Kırınımı Yöntemiyle C₁₂H₁₀N₄O₄S₂, C₁₆H₁₈ClO₂PS ve C₁₇H₁₅ClO₃ Moleküllerinin Kristal Yapı Çözümü. Samsun: Doktora Tezi.
- Barbara, P. F., Rentzeper, L. E. & Brus, J. (1980). Photochemical kinetics of salicylidenaniline. Journal of American Chemical Society, 102, 2786-2791.
- Cogordan, J., Mayoral, M., Martinez, R., Toscano, A. & Angeles, E. (1998). Int. J. Quantum Chem., 71, 415-432.
- Chen, H. & Rhodes J. (1996). Schiff base forming drugs: mechenisms of immune potentiation and therapeutic potential. Journal of Molecular Medicine, 74, 497-504.
- Cohen, M. D., Schmidt, G. M. J. & Flavain, S. (1964). Experiments on photochromy and thermochromy of crystalline anils of salicylaldehydes. Journal of Chemical Society, 388, 2041-2051.
- Çetinkaya, B., Binbaşoğlu, B., Özdemir, I., Ülkü, D., Tahir, M. N. & Arıcı, C. (In press).

Çetinkaya, B., Çetinkaya, E., Küçükbay, H. & Durmaz, R. (1996). Arzneim.-Forsch./Drug Res., **46**, 1154.

Dey, D. K., Dey, S. P., Elmali, A. & Elerman, Y. (2001). Molecular structure and conformation of N-2-[3¹-(methoxysalicylideneimino)benzyl]-3^{''}-methoxy salicylideneimine. Journal of Molecular Structure, **562**, 177-184.

Elmali, A., Elerman, Y. & Zeyrek, C. T. (1998). Conformational study and structure of N-(2,5-methylphenyl)salicylaldimine. Journal of Molecular Structure, **443**, 123-130.

Elmali, A., Kabak, M. & Elerman, Y. (1999). Conformation and structure of 3-methoxyphenyl-salicylaldimine. Journal of Molecular Structure, **484**, 229-234.

Elmali, A. & Elerman, Y. (1998). Structure and conformation of N-(2-methyl-5-chlorophenyl)salicylaldimine. Journal of Molecular Structure, **442**, 31-37.

Farrugia, L. J. (1997). Ortep3 for Windows. Journal of Applied Crystallography, **30**, 565.

Farrugia, L. J. (1999). WinGX. Journal of Applied Crystallography, **32**, 837-838.

Fernandez-G, J. M., del Rio-Portilla, F., Quiroz-Garcia, B., Toscano, R. A. & Salcedo, R. (2001). The structures of some ortho-hydroxy Schiff base ligands. Journal of Molecular Structure, **561**, 197-207.

Filarowski, A., Glowiake, T. & Koll, A. (1999). Strengthening of the intramolecular O...H...N hydrogen bonds in Schiff bases as a result of steric repulsion. Journal of Molecular Structure, **484**, 75-89.

Giacovazzo, C. (1998). Fundamentals of Crystallography. Oxford: Oxford University Press.

- Hadjoudis, E., Vittorakis, M. & Moustakali-Mavridis, I. (1987). Photochromism and thermochromism of Schiff bases in the solid state and in rigid glasses. Tetrahedron, **43**, 1345-1360.
- Hadjoudis, E. (1981). Photochromism and thermochromism of N-salicylidene anilines and N-salicylideneaminopyridines. Journal of Photochemistry, **17**, 355-363.
- Insuasty, B., Rodrigues, R., Quiroga, J., Abonia, R., Martinez, R., Toscano, A. & Angeles, E. (2001). Synthesis of 1-Benzyl-6-(4-chlorophenyl)-2-(4-R-phenyl)-4-(4-R-styryl)-2,3-dihydropyrazolo[3,4-b]diazepines. Molecules, **6**, 710-715.
- Kazak, C. Aygün, M., Turgut, G., Odabaşoğlu, M., Özbey, S. & Büyükgüngör, O. (2000). 2-[(4-hydroxyphenyl)iminomethyl]thiophene. Acta Crystallographica, **C56**, 1044-1045.
- Lappert, M. F. (1988). Journal of Organometallic Chemistry, **358**, 185.
- Ladd, M. F. C. & Palmer, R. A. (1988). Structure Determination by X-Ray Crystallography. (2nd ed.). New York, London: Plenum Press.
- Lecture Notes for the Tenth Summer School "Course In Crystallography". (2001). Structure Analysis by X-Ray Crystallography. (4th ed.). American Crystallographic Association: University of Georgia, USA.
- Martinez, R., Angeles, E. & Hernandez, P. E. (1996). Heterocyclic variants of 1,5-benzodiazepine system 7. Synthesis of substituted 2a-phenyl-4-methylsulfonyl-2-methoxy-1,2,2a,3-tetrahydroazeto[1,2-a][1,5]benzodiazepin-1-ones. Heterocycles, **33**, 271-274.

- Nazır, H., Yıldız, M., Yılmaz, H., Tahir, M. N. & Ülkü, D. (2000). Intramolecular hydrogen bonding and tautomerism in Schiff bases, Structure of N-(2-pyridil)-2-oxo-1-naphthylidenemethylamine. Journal of Molecular Structure, 524, 241-250.
- Ochoa, M. E., Rojas-Lima, S., Höpfl, H., Rodriguez, P., Castillo, D., Farfan, N. & Santillan, R. (2001). Facile synthesis of 1,3,6-oxadiazepines from 2,2'-(1,2-ethanediyldiimino)bisphenols. Tetrahedron, 57, 55-64.
- Sabatie, A., Vegh, D., Loupy, A. & Floch, L. (2001). Synthesis of aromatic and heteroaromatic annelated [1,4]diazepines. ARKIVOC, vi, 122-128.
- Sandler, S. R. & Karo, W. (1986). Organic Functional Group Preparations. (Vol.11). New York: Academic Press.
- Schmidt, G. M. J., in: Ginsburg, D. (Ed.). (1976). Solid State Photochemistry. New York, Weinheim: Verlag Chemie.
- Sheldrick, G. M. (1998). SHELXS-97, A program for crystal structure solution, University of Göttingen, Germany.
- Sheldrick, G. M. (1998). SHELXL-97, A program for crystal structure refinement, University of Göttingen, Germany.
- Spek, A. L. (1990). Platon-Pluton. Acta Crystallographica, A46, C34.
- Wafai, Z. A. & Mehta, V. L. (1986). Some neuropharmacological actions of 3-methyl-5-phenyl-(4'-methyl)-quinolenodiazepine. Indian Journal of Pharmacology, 18, 89-94.
- Winberg, H. E., Downing, J. R. & Coffman, D. D. (1965). Journal of Am. Chem. Soc., 87, 2054.

Williams, D. R. (1972). Metals, ligands, and cancer. Chemical Review, 72, 203-213.

Yang, F. & Hamilton, J. H. (1996). Modern Atomic and Nuclear Physics. New York: McGraw-Hill.

